



Influence of environmental parameters on the distribution of bacterial lipids in soils from the French Alps: Implications for paleo-reconstructions

Pierre Véquaud, Sylvie Derenne, Christelle Anquetil, Sylvie Collin, Jérôme Poulenard, Pierre Sabatier, Arnaud Huguet

► To cite this version:

Pierre Véquaud, Sylvie Derenne, Christelle Anquetil, Sylvie Collin, Jérôme Poulenard, et al.. Influence of environmental parameters on the distribution of bacterial lipids in soils from the French Alps: Implications for paleo-reconstructions. *Organic Geochemistry*, 2021, pp.104194. 10.1016/j.orggeochem.2021.104194 . hal-03157067

HAL Id: hal-03157067

<https://hal.science/hal-03157067>

Submitted on 4 Oct 2021

HAL is a multi-disciplinary open access archive for the deposit and dissemination of scientific research documents, whether they are published or not. The documents may come from teaching and research institutions in France or abroad, or from public or private research centers.

L'archive ouverte pluridisciplinaire **HAL**, est destinée au dépôt et à la diffusion de documents scientifiques de niveau recherche, publiés ou non, émanant des établissements d'enseignement et de recherche français ou étrangers, des laboratoires publics ou privés.

Influence of environmental parameters on the distribution of bacterial lipids in soils from the French Alps: Implications for paleo-reconstructions

Pierre Véquaud ^a, Sylvie Derenne ^a, Christelle Anquetil ^a, Sylvie Collin ^a, Jérôme Poulénard ^b,
Pierre Sabatier ^b, Arnaud Huguet ^{a*}

^a Sorbonne Université, CNRS, EPHE, PSL, UMR METIS, F-75005 Paris, France

^b Univ. Grenoble Alpes, Univ. Savoie Mont Blanc, CNRS, EDYTEM, F-73376 Le Bourget du
lac, France

Abstract

Branched glycerol dialkyl glycerol tetraethers (brGDGTs) are a family of bacterial lipids widely used for temperature and pH reconstructions in terrestrial settings. 3-hydroxy fatty acids (3-OH FAs) with 10 to 18 carbon atoms, produced by Gram-negative bacteria, have been recently proposed as independent and complementary proxies of temperature and pH in terrestrial environments. Nevertheless, the correlations between mean annual air temperature (MAAT)/pH and bacterial lipid (brGDGTs/3-OH FAs) distribution show a large degree of scatter, as the relative abundance of these lipids is influenced by factors other than temperature and pH. A full understanding of the environmental parameters influencing bacterial lipid distribution in soils is required to increase the reliability of the temperature and pH proxies based on these compounds in terrestrial environments. The aim of this work was to determine and quantify the cumulative effect of environmental parameters on the distribution of both brGDGTs and 3-OH FAs along a well-documented composite altitudinal transect in the French Alps (234-2,748 m). Redundancy analysis revealed that the influence of local parameters (pH and to a lesser extent soil moisture and grain size, related to vegetation and soil types) on brGDGT and 3-OH FA distribution amounted to 48.1% and 26.1%, respectively, and was predominant over MAAT. This likely explained the weak or lack of relationships between MAAT and brGDGT-/3-OH FA-based indices in this region. The identification of lipids whose fractional abundance is correlated with MAAT or pH allowed the development of local calibrations with MAAT/pH applicable in the French Alps which are representative of highly contrasted microenvironments, reflecting different types of soil and vegetation. The present study highlighted the importance of constraining the environmental factors affecting the

* Corresponding author. Tel: + 33-144-275-172; fax: +33-144-275-150.

E-mail address: arnaud.huguet@sorbonne-universite.fr (A. Huguet).

distribution of 3-OH FAs and brGDGTs in terrestrial settings prior to any paleoenvironmental reconstruction. Such an approach should be reproduced in other sites, where local factors could also strongly influence the bacterial lipid distribution.

Keywords: 3-hydroxy fatty acids; branched GDGTs; French Alps soils; altitudinal transect; environmental parameters; local calibration

1. Introduction

Direct measurement of environmental data, such as temperature and precipitation, has been possible for the last two centuries, the so-called "instrumental" period. Beyond this period, it is necessary to use indirect approaches to obtain information on the different environmental parameters. "Indirect" indicators of these parameters – so-called proxies – have thus been developed and used regularly for last decades.

Organic biomarkers have been of great interest to the scientific community for the reconstruction of past environments over the last decades (Eglinton and Eglinton, 2008), especially microbial compounds. Microorganisms modify the lipid composition of their membranes (e.g. carbon chain length, number of unsaturations, branching level) in response to variations of environmental parameters (pH, temperature, osmotic pressure) (Ernst et al., 2016). Such modifications are considered to maintain a functional fluidity and permeability of the microbial membrane (Singer and Nicolson, 1972; Sinensky, 1974; Hazel and Williams, 1990; Denich et al., 2003). These microbial lipids can be preserved in soils and sediments and be used as proxies of past environmental conditions.

In this context, glycerol dialkyl glycerol tetraethers (GDGTs) are a family of microbial lipids widely used for paleoenvironmental reconstructions. These compounds are ubiquitous in terrestrial (Weijers et al., 2007; Peterse et al., 2012; De Jonge et al., 2014; Naafs et al., 2017) and aquatic environments (Schouten et al., 2002, 2012; Powers et al., 2010; Peterse et al., 2015; Weber et al., 2015). They are characterized by aliphatic chains connected to two glycerol units via ether bonds. Two groups of GDGTs – isoprenoid and branched – can be distinguished (Schouten et al., 2013 and references therein). Isoprenoid GDGTs (iGDGTs) are produced by archaea. In contrast, GDGTs with branched chains but no isoprenoid alkyl chains – so-called branched GDGTs (brGDGTs) – are produced by still unidentified bacteria, although some of them may belong to the phylum *Acidobacteria* (Sinninghe Damsté et al., 2011, 2014, 2018). They were discovered in peat (Sinninghe Damsté et al., 2000). The analysis of brGDGTs in a

large number of soils distributed worldwide then showed that the relative distribution of these compounds is dependent on environmental parameters, mainly temperature and pH (Weijers et al., 2007; De Jonge et al., 2014, 2019).

Despite the wide application of brGDGT indices for paleoenvironmental reconstructions in terrestrial settings (Weijers et al., 2011; Wang et al., 2017; Coffinet et al., 2018), the derived results must be interpreted with caution, as parameters other than temperature or pH, such as humidity (Huguet et al., 2010; Menges et al., 2014), soil type (Davtian et al., 2016; Mueller-Niggemann et al., 2016), vegetation composition (Weijers et al., 2011; Naeher et al., 2014; Liang et al., 2019) or seasonality (Huguet et al., 2013) can also have an influence on the relative abundances of brGDGTs. These lipids are the only molecular proxies of temperature and pH available in the terrestrial environment to date, as most of the available proxies have been developed in oceanic environments. Despite improvements in brGDGT analytical methods and use of refined calibration models (De Jonge et al., 2014; Hopmans et al., 2016; Dearing Crampton-Flood et al., 2020), the Root Mean Square Error (RMSE) associated with Mean Annual Air Temperature (MAAT) reconstruction using the global brGDGT calibrations in soils remains high ($>4^{\circ}\text{C}$), possibly due to the lack of knowledge on all influencing environmental parameters. The development of new molecular proxies, independent of and complementary to brGDGTs, is essential to improve the reliability of environmental reconstructions in terrestrial settings.

Recent studies (Wang et al., 2016, 2018; Huguet et al., 2019; Yang et al., 2020) have unveiled the potential of another family of lipids – 3-hydroxy fatty acids (3-OH FAs) – for temperature and pH reconstructions. 3-OH FAs with 10 to 18 carbon atoms are specifically produced by all Gram-negative bacteria and are bound to the lipopolysaccharide (LPS; main component of the outer membrane) by ester or amide bonds. 3-OH FAs are part of the lipid A, which anchors the LPS in the outer membrane of Gram-negative bacteria. Three types of 3-OH FAs can be distinguished: with *normal* (i.e. straight and unbranched) or branched carbon chains, either *iso* or *anteiso*. These compounds were widely used (i) to quantify Gram-negative bacteria in clinical studies and detect the presence of endotoxins they release (Wollenweber and Rietschel, 1990; Saraf et al., 1997; Szponar et al., 2002, 2003; Keinänen et al., 2003) and (ii) to characterize and quantify Gram-negative bacteria communities in environmental samples such as aerosols (Lee et al., 2004; Cheng et al., 2012), dissolved organic matter (Wakeham et al., 2003), or soils (Zelles et al., 1995; Zelles, 1999).

3-OH FAs have been recently proposed as proxies of temperature and pH in terrestrial environments after analysis of these compounds in 26 soils along Mount Shennongjia, China

(Wang et al., 2016). New indices were developed, with RAN_{15} and RAN_{17} (defined as the ratio of C_{15} or C_{17} *anteiso* 3-OH FAs to *normal* C_{15} or C_{17} 3-OH FAs) being correlated with MAAT and RIAN (defined as $-\log ([normal\ 3-OH\ FAs]/[anteiso+iso\ 3-OH\ FAs])$) being dependent on soil pH.

Significant relationships between 3-OH FA distribution and temperature as well as pH were similarly observed along two additional altitudinal transects: Mount Majella in Italy and Mount Rungwe in Tanzania (Huguet et al., 2019). The RAN_{15}/RAN_{17} indices were negatively correlated to air temperature along the three mountains investigated so far (Wang et al., 2016; Huguet et al., 2019). This suggests that Gram-negative bacteria respond to colder temperatures with an increase in *anteiso*- C_{15}/C_{17} vs. *n*- C_{15}/C_{17} 3-OH FAs in order to maintain a proper fluidity and optimal state of the bacterial membrane, the so-called homeoviscous adaptation mechanism (Sinensky, 1974; Hazel and Williams, 1990). Nevertheless, the relationships between RAN_{15} and MAAT along Mts. Shennongjia, Rungwe and Majella showed the same slopes but different intercepts (Wang et al., 2016; Huguet et al., 2019), suggesting that regional calibrations may be more adapted to apply RAN_{15} as a temperature proxy in soils. In contrast, a significant ($R^2 = 0.60$) combined calibration between RAN_{17} and MAAT could be established using data from Mts. Shennongjia, Rungwe and Majella (Wang et al., 2016; Huguet et al., 2019). Similarly, RIAN was shown to be strongly negatively correlated with soil pH along the three aforementioned mountains (Wang et al., 2016; Huguet et al., 2019), reflecting a general relative increase in normal homologues compared to branched (*iso* and *anteiso*) ones with increasing pH. This mechanism was suggested to reduce the permeability and fluidity of the membrane for the cell to cope with lower pH (Watanabe and Takakuwa, 1984; Lepage et al., 1987; Russell, 1989; Russell et al., 1995; Denich et al., 2003; Beales, 2004). 3-OH FA indices were recently applied to estimate temperature and hydrological changes over the last 10,000 years in a speleothem from China (Wang et al., 2018), showing the potential of 3-OH FAs as independent tools for environmental reconstruction in terrestrial settings. A very recent study based on marine sediments from the North Pacific Ocean suggested that the distribution of 3-OH FAs could also be used to reconstruct sea surface temperature (Yang et al., 2020).

Even though these results are promising, the linear regressions between pH/MAAT data and 3-OH FA indices in terrestrial environments are still based on a rather small dataset (ca. 70 soil samples) and show a large degree of scatter, leading to substantial errors in 3-OH FA-based MAAT and pH reconstitutions ($MAAT-RMSE = 5.1^\circ C$; $pH-RMSE = 0.56$; Huguet et al., 2019). One can anticipate that the distribution of 3-OH FAs in soils is impacted by environmental parameters other than the temperature and pH, as observed for brGDGTs. A full

134 understanding of the environmental parameters (e.g. MAAT, pH, soil moisture, organic carbon
135 and nitrogen content, soil types and vegetation communities) influencing bacterial lipid
136 distribution (3-OH FAs and brGDGTs) in soils is required to increase the reliability of the
137 temperature and pH proxies. Nevertheless, to date, there is no report of a detailed investigation
138 of the environmental controls on 3-OH FA distribution in soils and only a limited number of
139 studies on brGDGTs address this question. The aim of this work is thus to determine and
140 quantify the cumulative effect of environmental parameters on the distribution of both
141 brGDGTs and 3-OH FAs along a composite altitudinal transect in a well-constrained sampling
142 site in the French Alps.

2. Material and methods

2.1. Sites and sampling

Surficial soil samples (0-10 cm depth) were collected in the French Alps in October 2017 along two well-documented (MAAT, soil types and vegetation composition) climate-toposequences: the Bauges massif between 232 and 1,475 m a.s.l (above sea level) and the Lautaret-Galibier massif between 1,540 and 2,700 m a.s.l. (Fig. 1; Supp. Fig. 1). MAAT and a precise description of soil types and vegetation composition are available in this area thanks to an integrated long-term observatory belonging to the Zone Atelier Alpes (Bounemoura al., 1998; Carlson et al., 2017; Choler, 2018). The Lautaret-Galibier and Bauges massifs cover a complementary range of altitude and make it possible to obtain a composite altitudinal transect that is representative of the variations in temperature, soil characteristics and plant communities in the French Alps (Table 1).

2.1.1. Bauges massif

Twenty-four soil samples were collected along the western slope of the Bauges massif (Fig. 2; Table 1). This massif, located in the north-western part of the French Alps, in the French National Park of the Bauges massif, is a low to medium altitude site (maximum altitude of 2,217 m a.s.l). To the north east, this massif is bordered by a group of mountains and the Annecy Lake. It is limited to the south west by the Bourget Lake. This is a carbonated subalpine massif, dominated by limestone chains oriented north-north-east / south-south-west. Their summits are mainly composed of Urgonian limestones. In the lower part of the massif, at an altitude of 200 m, the Mean Annual Precipitation (MAP, mm/years) is 1,221 mm and the MAAT 11.4 ° C (for the period 1981-2010, Chambéry meteorological station). In the upper part of the Bauges massif, at an altitude of around 1,300 m, the annual average rainfall is 1,704.9 mm and the MAAT 5.8 ° C (for the period 1981-2000, Feclaz weather station; Bounemoura al., 1998; Carlson et al., 2017; Choler, 2018).

The vegetation in the lower part of the massif is characterized by mountain ash tree (*Fraxinus excelsior*; around 200 m a.s.l.) and beech (*Fagus sylvatica*; between 900 and 1,000 m a.s.l) forest as well as meadows, dominated by *Carex foetida*. The higher part of the massif is characterized by heathland patchworks (*Vaccinium myrtillus* species, between 1,200 and 1,350 m a.s.l.) and coniferous forest (*Pinus sylvestris* around 1350 m; Fig. 2).

Soils in the lower part of the Bauges massif (around 200 m) are calcosols, influenced by the limestone bedrock. Within the beech forest, organosols are present on calcareous

substrates. Within the coniferous forest, soils are divided into patchworks of organosols – resulting from the accumulation of organic litter on calcareous substrates – and brunisols, mainly resulting from the accumulation of clays in topographic hollows (Table 1).

2.1.2. *Lautaret-Galibier massif*

Twenty-five soil samples were also collected in the Roche Noire high-elevation watershed, between 1,540 m and 2,700 m a.s.l (Fig. 2). The site is located in the Lautaret-Galibier Massif, which is part of the south-western Alps, between the passes of Lautaret (2,058 m a.s.l.) and Galibier (2,645 m a.s.l.). Average MAP along the Lautaret-Galibier massif is 1,300 mm and decreases with altitude. In the lower part of the massif, at an altitude of 1,500 m, MAAT is around 6°C. In the upper part of the massif, at an altitude of 2,700m, MAAT is around 0°C. Wooded vegetation, dominated by Larch forest (*Larix decidua*), occurs between 1,600 m and 1,900 m a.s.l. Heathlands dominated by *Vaccinium* spp. and grasslands dominated by the tall festuce *Patzkea paniculata* are observed between 1,900 m and 2,300 m a.s.l. The highest part of the site is dominated by a mosaic alpine meadow showing a high beta-diversity in plant vascular species in relation with mesotopographical variations (Choler, 2018)

Calcosols are found in the lowest part of the massif, between 1,500 and 2,000 m a.s.l., whereas subalpine grasslands and alpine meadows are dominated by brunisols. Alocrisols – developing on acidic rocks and intermediate between brunisols and podzolic soils – are also observed between 2,200 and 2,300 m a.s.l., as well as rendisols – poorly evolved and undifferentiated soils growing on calcareous substrates – at ca. 2,700 m a.s.l. and colluviosols – formed by slope deposits on pre-existing soils – at ca 2,500 m a.s.l (Table 1).

2.1.3. *Sampling*

Vegetation along the two massifs (Bauges and Lautaret-Galibier) is distributed in different biomes based on the thermal regime, but also precipitation and mesotopographical parameters. Therefore, three samples representative of the different soil types and/or vegetation were collected at each elevation. A total of 49 soil samples were collected (Table 1). After being transported to the laboratory, they were directly stored at -20 °C and then freeze-dried, ground and sieved at 2 mm.

2.1.4. *Temperature data*

Miniature temperature data loggers (Hobo Pendant UA, Onset Computer Corporation, Bourne, MA) were placed at 5 cm below the soil surface in 24 of the Bauges massif sites, allowing the daily measurement of the surface soil temperature. These temperatures are considered to be similar to MAAT and can be used as a first approximation as MAAT estimates (Bartlett et al., 2006; Weijers et al., 2007). The corresponding data were compiled for the period 2016-2018 and were completed by MAAT measurements from the Feclaz meteorological station (1,350 m a.s.l.). As no recorded temperature data were available for the 2016-2018 period along the Lautaret-Galibier massif, MAAT values from the Oisans massif, selected for its geographical and climatic proximity to the Lautaret-Galibier, were used instead, with 8 points distributed every 300 m between 750 and 3,550 m a.s.l. Data were provided by the SAFRAN-SURFEX/Crocus-MEPRA model chain (S2 M) developed by Météo France for the French Alps (Durand et al., 2009; Vionnet et al., 2012).

A linear regression was established between the available temperature data (Bauges and Oisans massifs as well as Feclaz station) and altitude (Supp. Fig. 2) to obtain a model allowing the reconstruction of MAAT at the different sampling sites (i.e. the whole composite transect along the Bauges and Lautaret-Galibier massifs). The MAAT values reported and discussed in the rest of the manuscript will be those obtained from this model ($R^2 = 0.97$; RMSE = 0.67 °C).

2.2. Bulk soil analyses

Soil water content (SWC) was determined by difference between the soil mass before and after freeze-drying.

The pH of the freeze-dried samples was measured in ultrapure water with a 1:2.5 soil water ratio. Typically, 10 ml of ultrapure water were added to 4 g of dry soil. The soil solution was stirred for 30 minutes, before decantation for 1 hour and pH measurement (Carter et al., 2007).

Soil samples were decarbonated before elemental (total organic carbon - Corg and nitrogen) and isotopic ($\delta^{13}\text{C}$ and $\delta^{15}\text{N}$) analyses following the protocol detailed by Huguet et al. (2013). Elemental and isotopic analyses were performed on the ALYSES platform (Sorbonne University / IRD) at Bondy, France. About 10 μg of decarbonated soil was typically weighed

in tin capsules before analyses using an Elementar Vario EL III (Elementar Analysensysteme GmbH, Germany)

The distribution of particle sizes into five sieved and crushed soil fractions – clays (< 2µm); fine silts (between 2 and 20 µm); coarse silts (between 20 and 50 µm); fine sands (between 50 and 200 µm) and coarse sands (between 200 and 2000 µm) – was determined at the Arras Soil Laboratory, France. The cation exchange capacity (CEC) was measured in the Arras Soil Laboratory using the METSON method (Metson, 1957).

2.3.brGDGT analysis

Sample preparation for brGDGT analysis was similar to that reported by Coffinet et al. (2014). Briefly, ca. 10 g of soil was extracted using an accelerated solvent extractor (ASE 100, Dionex-ThermoScientific, USA) with a dichloromethane (DCM) / methanol (MeOH) mixture (9: 1) for 3×5 minutes at 100 °C and a pressure of 100 bars in 34 ml cells. The total lipid extract was rotary evaporated and separated into two fractions of increasing polarity on a column of activated alumina: (i) 30 ml of heptane: DCM (9: 1, v:v) ; (ii) 30 ml of DCM: MeOH (1: 1, v:v). GDGTs are contained in the second fraction, which was rotary evaporated. An aliquot (300 µL) was re-dissolved in heptane and centrifuged using an Eppendorf MiniSpin centrifuge (Eppendorf AG, Hamberg, Germany) at 7000 rpm for 1 min.

GDGTs were then analysed by high pressure liquid chromatography coupled with mass spectrometry with an atmospheric pressure chemical ionisation source (HPLC-APCI-MS) using a Shimadzu LCMS 2020. GDGT analysis was performed using two Hypersil Gold silica columns in tandem (150 mm × 2.1 mm, 1.9 µm; Thermo Finnigan, USA) thermally-controlled at 40 °C, as described by Huguet et al. (2019). This methodology enables the separation of 5- and 6-methyl brGDGTs. Semi-quantification of brGDGTs was performed by comparing the integrated signal of the respective compound with the signal of a C₄₆ synthesized internal standard (Huguet et al., 2006) assuming their response factors to be identical.

The MBT'_{5Me} index, reflecting the average number of methyl groups in 5-methyl isomers of GDGTs and considered as related to MAAT, was calculated according to De Jonge et al. (2014; Eq. 1; Supp. Data):

$$\text{MBT}'_{5\text{Me}} = \frac{[Ia+Ib+Ic]}{[Ia+Ib+Ic] + [IIa+IIb+IIc] + [IIIa]} \quad (1)$$

The CBT index, reflecting the average number of cyclopentyl rings in GDGTs and considered as related to pH, was calculated as follows (Peterse et al., 2012; Eq. 2; Supp. Data):

$$CBT = -\log \left(\frac{[Ib] + [IIb + IIb']}{[Ia] + [IIa + IIa']} \right) \quad (2)$$

The Roman numerals correspond to the different GDGT structures presented in De Jonge et al. (2014). The 6-methyl brGDGTs are denoted by an accent after the Roman numerals for their corresponding 5-methyl isomers. Analytical errors associated with the calculation of MBT'_{5Me} and CBT indices are respectively 0.03 and 0.04 based on the analysis of 5 samples in triplicates among the 49 soil samples.

2.4. 3-OH FA analysis

Sample preparation for 3-OH analysis was identical to that reported by Huguet et al. (2019). 10 g of freeze-dried soil were subjected to acid hydrolysis (reflux with 30 ml of 3M HCl in a 130 °C silicon oil bath for 3 hours). The suspension was then centrifuged at 15 °C and 3000 rpm for 10 minutes. The supernatant was collected in an Erlenmeyer flask. The residue was then ultrasonically extracted with a mixture of DCM:MeOH (1:1, v/v; 2× ; 20 ml) and DCM (2× ; 20 ml). Each extraction was followed by centrifugation and pooling of all extracts. The DCM phase was then separated from the MeOH/H₂O layer, which was again extracted with DCM (3 times; 20 ml). This DCM fraction was then rotary-evaporated, methylated in a 1M HCl-MeOH solution at 80 °C for 1 hour and separated into three fractions over an activated silica column: (i) 30 ml of heptane/EtOAc (98: 2), (ii) 30 ml of EtOAc and (iii) 30 ml of MeOH. 3-OH FAs contained in the second fraction were derivatised with a solution of *N,O*-bis(trimethylsilyl)trifluoroacetamide (BSTFA) – Trimethylchlorosilane (TMCS) 99:1 (Grace Davison Discovery Science, USA) before gas chromatography-mass spectrometry (GC-MS) analysis.

3-OH FAs were analysed with an Agilent Network 6980 GC-MS using a Restek RXI-5 Sil MS silica column (60 m × 0.25 mm, i.d. 0.50 µm film thickness), as previously described (Huguet et al., 2019). 3-OH FAs were quantified by integrating the appropriate peak (*m/z* = 175) on the ion chromatogram and comparing the area with an internal standard (3-hydroxytetradecanoic acid, 2,2,3,4,4-d₅; Sigma-Aldrich, France). The internal standard (0.5 mg/ml) was added just before injection as a proportion of 3 µl of standard to 100 µl of sample, as detailed by Huguet et al. (2019). The different 3-OH FAs were identified based on their retention time, after extraction of the characteristic *m/z* 175 fragment (*m/z* 178 for the deuterated internal standard; cf. Huguet et al., 2019).

The RIAN index was calculated as follows (Wang et al., 2016; Eq. 3) in the range C₁₀-C₁₈ (Supp. Data):

$$RIAN = -\log[(I + A)/ N] \quad (3)$$

where I, A, N represent the sum of all *iso*, *anteiso* and *normal* 3-OH FAs, respectively.

RAN₁₅ and RAN₁₇ indices are defined as follows (Wang et al., 2016; Eqs. 4 and 5; Supp. Data):

$$RAN_{15} = [\textit{anteiso} C_{15}] / [\textit{normal} C_{15}] \quad (4)$$

$$RAN_{17} = [\textit{anteiso} C_{17}] / [\textit{normal} C_{17}] \quad (5)$$

Analytical errors associated with the calculation of RIAN, RAN₁₅ and RAN₁₇ indices are respectively 0.009, 0.19 and 0.06 based on the analysis of one sample injected eleven times during the GC-MS analysis.

2.5. Statistical analysis

In order to investigate the correlations between the different environmental variables (soil moisture, pH, MAAT, Corg and N contents) and the relative abundances of membrane lipids (brGDGTs and 3-OH FAs), pairwise correlation matrices were performed in addition to single or multiple linear regressions. As the majority of variables are not normally distributed (except for δ¹⁵N and clay content), Spearman correlation was used with a confidence level of 5%. Linear regressions and correlation matrices were performed with R software, version 3.6.1 (R Core Team, 2014).

Redundancy analysis (RDA) was performed on the 49 soil samples to identify the relationships between environmental variables and 3-OH FA or brGDGT distribution. RDA is a "constrained" analysis, used to directly visualize the variation in the lipid data as a function of the environmental variables. Redundancy analysis allows not only assessing but also quantifying the influence of each explanatory variables (i.e. environmental variables) on the distribution of bacterial lipids. RDA analysis yields the influence of each variable, with regards to the statistical variance, on the pool of bacterial lipids, and allowed a quantification in percent of the influence of each parameter. The quantification of the effect of each variable can be considered in two ways. Simple (or marginal) effects are the effects of each variable considered independently of the other variables. Conditional effects summarize the effects of each variable taking into account the effect of variables with a greater influence (Braak and Smilauer, 2002). A forward selection was performed using the Canoco software (v. 5.04) to help in the selection of the best subset of the variables explaining the variation in 3-OH FA and brGDGT distributions. RDA analyses were performed on centered and standardized data using the

338 CANOCO v. 5.04 software (Braak and Smilauer, 2002). The relationships between each
339 variable and the dimensions of the RDA were investigated using the corresponding r-values
340 and the percentages of variance.
341

3. Results

3.1. Bulk soil properties

The organic carbon content (C_{org}) shows a wide range of variation – from 1.4% for poorly evolved soils (lithosol) to 49.10% for forest organosol (litter soil) – with an average of 9.7% and a standard deviation of 10.3% (Table 2). Only a minority of soils ($n = 4$) display high C_{org} values ($> 30\%$). The $\delta^{13}C$ values show a unimodal distribution ($-26.7\text{‰} \pm 2.3\text{‰}$) and range between -29.9‰ and -24.4‰ (Table 2). The N content of the soil samples is normally distributed ($0.7\% \pm 0.5\%$; Table 2). Relative soil moisture is unimodally distributed and largely varies between soils, ranging between 3.4 and 68.2% (mean $30.3\% \pm 15.6\%$; Table 2). With regard to the texture of the sampled soils, the clay contents are on average 313.8 ± 126.7 g/kg of soil and largely vary between samples (minimum and maximum values of 33 and 546 g/kg of soil, respectively). This large variability of the soil characteristics is also reflected in the silt (406.4 ± 117.0 g/kg soil) and sand (279.8 ± 194.1 g/kg soil) contents, as well as in the CEC values (24.2 ± 17.0 cmol $+/kg$; Table 2). Finally, the pH values show a wide range of variation (3.62–7.49), with an average of 5.83 and a standard deviation of 1.08.

3.2. BrGDGT and 3-OH FA distribution

3-OH FAs and brGDGTs were detected in the 49 studied soil samples (Supp. Tables 1 and 2). BrGDGT distribution was dominated by acyclic compounds (Ia, IIa, IIa', IIIa, IIIa') which represent in average ca. 80% of total brGDGTs (Fig. 3a). BrGDGTs Ia and IIa were the most abundant homologues in all samples. The pentamethylated brGDGTs (IIa-c; mean 50%, standard deviation (SD) of 6.9%) were predominant over the tetramethylated (Ia-c) and hexamethylated (IIIa-c; Fig. 3a). The 5-methyl isomers were present in higher proportion (mean 74%, SD 15.6%) than the 6-methyl compounds (mean 26%, SD 15%) (Fig. 3a).

3-OH FAs with chain lengths between 8 and 26 C were identified. These compounds may have various origins depending on their chain length (bacteria, plants and fungi; Zelles et al., 1999; Wang et al., 2016 and reference therein). Nevertheless, most of the 3-OH FAs present in our samples are homologues with 10 to 18 C atoms, generally associated with Gram-negative bacteria (Saraf et al., 1997; Szponar et al., 2002, 2003; Keinänen et al., 2003) and only these homologues will be considered in the following. 3-OH FAs with even carbon number and *normal* chains were the most abundant compounds in all samples (about 65% of the 3-OH FAs, SD 12%), with a predominance of the *n*-C₁₄ homologue (Fig. 3b). *Iso* (mean 24%, SD 4.5%)

and *anteiso* (mean 8%, SD 1%) isomers were also present. It must be noted that *anteiso* isomers were only detected for odd 3-OH FAs (Fig. 3b).

4. Discussion

The distribution of brGDGTs (Weijers et al., 2007, Peterse et al., 2012; De Jonge et al., 2014) and 3-OH FAs (Wang et al., 2016; Huguet et al., 2019) in soils was reported to be influenced mainly by MAAT and soil pH. Therefore, the effect of these two environmental parameters on the relative abundance of 3-OH FAs and brGDGTs in the 49 soils of the French Alps was first investigated.

4.1. BrGDGTs and 3-OH FAs as proxies of pH and temperature

4.1.1. Relationship between pH and bacterial lipid distribution

BrGDGT-derived CBT index has been shown to be strongly correlated with pH in a large set of globally distributed soils (De Jonge et al., 2014; Naafs et al., 2017). Consistently, in the French Alpine soils, CBT displayed a significant ($p < 0.05$) and strong correlation ($R^2 = 0.85$; RMSE = 0.42) with soil pH (Fig. 4a), in accordance with the global CBT-pH calibration proposed by De Jonge et al. (2014). This confirms the robustness of the CBT as a soil pH proxy taking into account the highly contrasting environmental characteristics of these French Alps soils.

The soils of the French Alps (Table 2) and those of Mts. Rungwe, Majella and Shennongjia, previously investigated for 3-OH FA distribution (Wang et al., 2016; Huguet et al., 2019), cover a similar range of pH (ca. 3–8) and of RIAN index (0.13–0.55 in the French Alps, Table 2; 0.15–0.70 for the other soils, Wang et al., 2016; Huguet et al., 2019). In the French Alps, the RIAN index was observed to be moderately ($R^2 = 0.43$; RMSE = 0.83) but significantly negatively correlated ($p < 0.001$) with soil pH (Fig. 4b), consistent with the significant correlation observed along the previously investigated altitudinal transects (Wang et al., 2016; Huguet et al., 2019). This confirms the general influence of pH on the relative abundance of 3-OH FAs in soils.

Nevertheless, a stronger correlation between RIAN and pH ($R^2 = 0.62$) was obtained for the dataset combining soils from Mts. Rungwe, Majella and Shennongjia (Huguet et al., 2019) compared to the one from the French Alps. In addition, the RIAN-pH correlations along the French Alps (Fig. 4b) and along Mts. Rungwe, Majella and Shennongjia (Huguet et al., 2019) displayed significantly different slopes and intercepts (p -value = 0.049), reflecting local

trends between 3-OH FA distribution and pH. Finally, the scatter in the RIAN-soil pH relationship along the French Alps (Fig. 4b), reflected in the average value of the prediction interval (0.35), suggests that parameters other than pH also affect the distribution of 3-OH FAs along this transect.

4.1.2. Relationship between MAAT and bacterial lipid distribution

In addition to pH, the relationship between bacterial membrane lipid distribution and MAAT was also investigated. BrGDGT-based MBT'_{5Me} was significantly ($p < 0.001$) negatively correlated with MAAT in the French Alps (Fig. 5a). Nevertheless, this correlation was substantially weaker ($R^2 = 0.35$) than the one between MAAT and MBT' or MBT'_{5Me} for (i) soils distributed worldwide ($R^2 = 0.66$; De Jonge et al., 2014) and (ii) along other altitudinal transects: Mount Kilimanjaro, Tanzania ($R^2 = 0.75$; Sinninghe Damsté et al., 2008); Mount Xiangpi, China ($R^2 = 0.64$; Liu et al., 2013); Mount Rungwe, Tanzania ($R^2 = 0.74$; Coffinet et al., 2014); Andean transect, Colombia ($R^2 = 0.67$; Anderson et al., 2014), East Coast of the USA ($R^2 = 0.47$; Dirghangi et al., 2013). The lower RMSE in this study (3.3 °C), in comparison with the RMSE of the global calibration (4.8 °C) could be partly explained by the relatively small number of samples ($n = 49$) analyzed within the French Alps, compared to the global dataset ($n = 231$) presented by De Jonge et al. (2014). Even though the relationship between brGDGT distribution and MAAT is generally strong, there is a substantial scatter in the MBT'_{5Me}-MAAT global calibration, leading to the high RMSE mentioned above (De Jonge et al., 2014), which reflects the heterogeneous and local response of brGDGT distribution to temperature. Such heterogeneity is also visible at the regional level, with e.g. significant differences in the relationship between brGDGT distribution and MAAT/soil pH along several altitudinal transects subjected to different precipitation regimes (Anderson et al., 2014). The weak relationship between MBT'_{5Me} and MAAT in the French Alps, associated with an uncertainty (RMSE) of 3.3 °C, reflects the fact that local parameters other than MAAT should be the primary controls of 5-methyl brGDGT relative abundance along this specific transect.

Regarding 3-OH FAs, the temperature proxies based on these compounds, namely RAN₁₅ and RAN₁₇, did not show any correlation with MAAT in the French Alps (Fig. 5b, c). In contrast, significant negative correlations between RAN₁₅ and MAAT were previously observed along Mt. Shennongjia ($R^2 = 0.51$; Wang et al. 2016), Mt. Rungwe and Mt. Majella ($R^2 = 0.80$; $p < 0.001$ and $R^2 = 0.54$; $p = 0.01$, respectively; Huguet et al., 2019) with similar slopes but different intercepts. This was interpreted as the result of local effects on RAN₁₅, despite a similar general response to temperature changes (Huguet et al., 2019). As observed for RAN₁₅,

RAN₁₇ was significantly negatively correlated with MAAT along Mt. Shennongjia ($R^2 = 0.48$; Wang et al. 2016), Rungwe and Majella ($R^2 = 0.54$ and 0.28 , respectively; Huguet et al., 2019) with similar slopes and ordinates, showing a comparable response of RAN₁₇ to temperature variations in these different locations. Nevertheless, there was only a weak correlation between RAN₁₇ and MAAT along Mt. Majella (Huguet et al., 2019), characterized by the closest altitudinal, geographical and climatic conditions to those of the French Alps in comparison with other investigated mountains. This result, combined with the absence of correlation between either RAN₁₅ or RAN₁₇ and the MAAT in the French Alps (Fig. 5b), suggests that locally the relative abundance of C₁₅ and C₁₇ 3-OH FAs may be mainly influenced by environmental parameters other than MAAT.

The Bauges and Lautaret-Galibier massifs, investigated in the present study, are a combination of highly diverse microecosystems resulting from microtopographical and geological (nature of the bedrock) differences and characterized by specific vegetation and soil types, precipitation or snow cover. This multiplicity of environmental variables may therefore affect the distribution of bacterial lipids in soils, as previously shown for brGDGTs (e.g. soil moisture, Dirghangi et al., 2013; granulometry, Peterse and Eglinton, 2017; vegetation or soil type, Davtian et al., 2016, Liang et al., 2019). This might reflect either changes in bacterial communities as previously reported (Hofmann et al., 2016; Siles and Margesin, 2016; Shen et al., 2019) and/or adaptation mechanisms of a constant community. Statistical analyses were performed to disentangle and quantify the main drivers of changes in bacterial lipid distribution along the Bauges and Lautaret-Galibier massifs and thus explain the weakness or lack of correlations of the 3-OH FA-/brGDGT-derived proxies with MAAT.

4.2. Impact of other environmental variables on bacterial lipid distribution

4.2.1. Selection of non-redundant environmental variables for statistical analyses

Before constraining the influence of the different environmental factors on 3-OH FA and brGDGT distribution using redundancy analyses (RDA), non-redundant environmental variables, which carry significantly different information, had to be selected. To this aim, a Spearman correlation matrix was first computed (Fig. 6), allowing the determination of the correlations between the different environmental variables. Highly correlated variables can be considered as redundant. Only correlation coefficients with red (negative correlation) or blue (positive correlation) colors are statistically significant ($p < 0.05$) (Fig. 6).

As MAAT values were reconstructed using a linear model with altitude (cf. section 2.1.4.), MAAT and altitude were logically anticorrelated along the Bauges and Lautaret-

Galibier, reflecting the natural cooling of air with elevation (Fig. 6). Altitude (and thus MAAT) was moderately correlated with soil pH ($r = -0.44$) and strongly correlated with $\delta^{13}\text{C}$ ($r = 0.77$). A relationship between soil pH and altitude was similarly observed along other altitudinal gradients but the sign of the correlation was shown to be strongly site-dependent (Cheng- Jim et al., 2014; Bhandari et al., 2019). It can be influenced by multiple factors such as soil types, source rock (e.g. calcareous or granitic) or vegetation composition (e.g. presence or absence of conifers; Smith et al., 2002; Djukic et al., 2010; Gutiérrez-Girón et al., 2015). Similarly, the relationship between $\delta^{13}\text{C}$ and altitude could be due to different vegetation, litter input and degradation of OM with thermal regimes, as suggested along other mountains (Wei et al., 2009; Du et al., 2014). Indeed at higher altitudes, the degradation of OM may be reduced, in contrast with the lower altitudes and higher temperatures, where plant accumulation is higher than decomposition (Davidson and Janssen, 2006; Conant et al., 2011).

Altitude is correlated to a set of environmental parameters, such as MAAT, carbon content, pH and can be considered as an integrative variable of the changes in vegetation, soil and relief types. In order to observe the sole effect of MAAT variation on brGDGT and 3-OH FA distribution, MAAT rather than altitude was kept as a non-redundant parameter. The $\delta^{15}\text{N}$ of the different soil samples showed moderate correlations ($r < 0.7$) with six of the eleven parameters investigated (Fig. 6) and was therefore considered as a confounding parameter. Organic carbon content (C_{org}) of the soils was observed to be strongly correlated with the nitrogen content ($r = 0.97$) and $\delta^{15}\text{N}$ ($r = -0.53$) as well as with the cation exchange capacity ($r = 0.73$; Fig. 6). C_{org} was also moderately correlated with soil water content ($r = 0.64$) and soil clay content ($r = 0.54$; Fig. 6) and was therefore considered as a redundant variable in the present study. Similarly, based on collinearity relationships with other variables, N content, $\delta^{15}\text{N}$ and CEC will not be considered in the following statistical tests. In order to confirm the choice of the non-redundant variables for RDA analyses made using the Spearman correlation matrix (Fig. 6) and determine the best set of variables explaining the distribution of brGDGTs/3-OH FAs, a forward selection analysis was performed through the Canoco software. This highlighted MAAT, pH, soil moisture, sand and clay contents (reflecting the grain size gradient of the soil) as explanatory variables, in line with Spearman correlation tests (Fig. 6).

The choice of these variables for subsequent RDA analysis is not unexpected, as MAAT and pH were shown to have a major influence on bacterial communities, which develop adaptation mechanisms to cope with variations of such parameters (Denich et al., 2003; Beales, 2004; Fierer and Jackson, 2006). This is especially the case for brGDGT- and 3-OH FA-producing bacteria (De Jonge et al., 2019; Huguet et al., 2019). Similarly, soil moisture may

affect the relative abundance of bacterial membrane lipids, as shown for brGDGTs (e.g. Peterse et al., 2012; Dirghangi et al., 2013; Ding et al., 2015). Soil moisture varies, as a first approximation, according to the precipitation regime, but it can also be related to other factors such as evapotranspiration, grain size or vegetation cover (Crave and Gascuel-Oudou, 1997; Gómez-Plaza et al., 2001). The grain size gradient is representative of the edaphic parameters which may influence bacterial diversity in soils (Hemkemeyer et al., 2018) in relationship with changes in soil (micro)structure and organic matter availability and which may also in turn affect the distribution of 3-OH FA and brGDGT source microorganisms in soils, as proposed below.

Selecting only non-redundant variables for RDA simplifies the analysis and makes it more robust. Nevertheless, RDA analyses carried out with all the variables, confirmed that MAAT, pH and soil moisture were the parameters mainly influencing 3-OH FA and lipid distribution (data not shown). Therefore, in the following, we will only discuss the results of the RDA analyses performed with the aforementioned non-redundant variables.

4.2.2. RDA analysis of brGDGT distribution and environmental variables

Regarding the RDA related to brGDGTs (Fig. 7a, Table 3), the first two axes explain 50.2 % of the total inertia of the dataset. The selected environmental variables are sufficient to explain 89.4 % of the variance in the brGDGT relative abundance (referred to as explained fitted variation in Table 3). On the first axis, the RDA analysis shows a predominant effect of pH ($r = 0.96$; Table 3) and a weaker contribution of MAAT ($r = 0.71$) and soil moisture ($r = -0.26$) on the distribution of brGDGTs. Axis 2, on the other hand, is influenced by MAAT ($r = 0.62$), relative soil moisture ($r = 0.53$) and to a lesser extent by pH ($r = -0.26$) and soil texture parameters, with a positive correlation with the sand content ($r = 0.08$) and a negative one with the clay content ($r = -0.20$; Fig. 7a and Table 3).

To go further, the influence of each environmental variable on the relative distribution of brGDGTs can be quantified through RDA analysis (Table 4). When the effect of each variable is considered individually, the influence of pH on brGDGT distribution appears predominant (41.1 %), followed by MAAT (25.2 %) and to a lesser extent soil moisture (5.3 %; Table 4). This is in line with observations made from the global soil dataset by De Jonge et al. (2014), where the variance of the relative abundances of the 15 individual brGDGTs in 231 soils was investigated using a Principal Component Analysis (PCA). When the first two components of this PCA are considered, it appears that pH was positively correlated with the

largest component of the variance (40 %), while MAAT and MAP were correlated together with the other component (17 %).

In the natural environment, environmental parameters do not influence bacterial lipid distribution separately, but are interrelated and act concomitantly, with e.g. soil moisture impacting the capacity of a soil to retain heat, thus indirectly influencing the temperature (Idso et al., 1975; Davidson et al., 1998). Therefore, the combined effect of the different environmental variables on brGDGT distribution was also investigated statistically. The conditional influence of these variables (Table 4) on the brGDGT distribution shows once again a clear predominance of the effect of pH (41.1 %), with a reduced influence of temperature (8.1 %), particle size (5.5 %) and soil moisture (1.5 %; Table 4). pH, grain size (clay/sand) content and soil moisture can be all considered as variables related to the local environment, i.e. microtopography, vegetation cover and soil type. When combined together, the influence of these local parameters on brGDGT distribution amounts to 48.1 % against only 8.1 % for MAAT (Table 4), which can explain the weakness of the MBT'_{5Me}-MAAT relationship in soils from the French Alps and its large degree of scatter (Fig. 5a).

The RDA triplot also illustrates the influence of the different environmental variables on the relative abundance of the individual brGDGTs (Fig. 7a). BrGDGTs comprising cyclic moieties (i.e with subscript b or c) are strongly and mainly positively correlated with the first axis of the RDA, and thus positively correlated with pH. As most of these cyclic compounds are used in the calculation of the CBT index, this explains the strong correlation between CBT and pH observed in the soils of the French Alps ($R^2 = 0.85$; Fig. 4a), consistent with the trends observed in soils distributed worldwide (De Jonge et al., 2014). In contrast with cyclic brGDGTs, acyclic 5-methyl brGDGTs (with subscript a) are located in the left half of the RDA (Fig. 7a) and show a moderate to strong correlation with the second axis of the RDA, especially brGDGT IIIa which is highly negatively influenced by MAAT. However, except compound IIIa, all the brGDGTs involved in the calculation of the MBT'_{5Me} are more influenced by pH than by temperature (Fig. 7a), hence a rather moderate correlation between this index and MAAT ($R^2=0.35$; Fig. 5a) is observed. Therefore, in contrast with previous studies where 5-methyl brGDGT distribution in soils was suggested to be mainly affected by MAAT and to a lesser extent by soil pH (De Jonge et al., 2014, Naafs et al., 2017), the relative abundance of the 5-methyl brGDGTs in the soils from the French Alps seems to be mainly driven by soil pH, with only compound IIIa showing a strong correlation with MAAT (Fig. 7a). This may be related to a recent study by De Jonge et al. (2019), which highlighted the strong effect of pH on brGDGT distribution in addition to MAAT, with a different pH-dependency in soils from warm

and cold environments. As for the 6-methyl brGDGTs, located in the right part of the RDA (Fig. 7a), their relative abundance in the soils of the French Alps appear well-correlated with pH, as observed in a large set of globally distributed soils ($n = 350$) by Naafs et al. (2017). BrGDGT distribution is only weakly influenced by soil moisture (especially compound Ia) and soil texture in soils from the French Alps (Fig. 7a).

4.2.3. RDA analysis of 3-OH FA distribution and environmental variables

Similarly to brGDGTs, RDA analysis was performed to investigate the effect of the different environmental parameters on 3-OH FA distribution (Fig. 7b). The first two axes of the RDA explain 31.8 % of the total inertia of the dataset. The explained fitted variation represents 81.2 % of the total inertia of the relationship between 3-OH FAs and the environmental variables (Table 3). The RDA analysis shows a predominant contribution of pH ($r = 0.95$), positively correlated with axis 1, on the distribution of 3-OH FAs (Fig. 7b, Table 3). Soil moisture ($r = -0.56$) MAAT ($r = 0.29$), sand content ($r = -0.21$) and clay content ($r = -0.32$) show a weaker correlation with the axis 1. Axis 2 is mainly related to the MAAT ($r = -0.93$), to the relative soil moisture ($r = -0.41$; Fig. 7b, Table 3) and to a lesser extent with pH ($r = 0.23$). Soil structure parameters (sand and clay contents) are poorly represented on the axis 2 of the RDA. (Fig. 7b; Table 3).

These qualitative trends are confirmed after quantification of the influence of each environmental variable on 3-OH FA distribution (Table 4). The study of simple effects also shows a predominant influence of pH on 3-OH FA distribution (20.0 %) followed by relative soil moisture (9.9 %), temperature (11.2 %) and particle size (3.8%). The combined influence of the different variables on the 3-OH FA relative abundance shows similar results, with pH (20.0 %) and to a lesser extent temperature (10.9 %) and soil moisture (3.6 %) being the main parameters affecting the lipid distribution (Table 4). Like brGDGTs, the influence of local parameters related to soil type and vegetation (i.e. soil pH, grain size content and soil moisture) on 3-OH FA distribution is predominant (26.1 %; Table 4) over MAAT, which could explain the absence of correlation between 3-OH FA distribution, especially RAN₁₅, RAN₁₇ indices and MAAT (Fig. 5b, c).

When considering the relative abundances of the individual 3-OH FAs in the RDA, it appears that most 3-OH FAs are grouped in a narrow sector of the circle (Fig. 7b). They encompass compounds with branched chains (*anteiso*-C₁₁, *iso*-C₁₂, *iso*-C₁₃, *anteiso*-C₁₃, *iso*-C₁₄, *anteiso*-C₁₅, *iso*-C₁₆, *iso*-C₁₇, *anteiso*-C₁₇), but also *normal* ones (C₁₅, C₁₇). This sector is close to the positive part of the first axis and thus these compounds are mostly influenced by pH. In

contrast, this sector appears orthogonal to MAAT and opposite to soil moisture. Outside this sector, the *normal* C₁₄ 3-OH FA is negatively correlated with the first axis and the *iso* C₁₅ on the one hand and the *normal* C₁₀ and C₁₁ on the other hand are respectively positively and negatively correlated with the MAAT (Fig. 7b).

The predominant influence of pH on the relative abundance of all *iso*, *anteiso* and *normal* 3-OH FAs except the *iso* C₁₅, *normal* C₁₈ and *normal* C₁₀ homologues (Fig. 7b) explains the existence of a relationship between the RIAN index and pH (Fig. 4b). Nevertheless, this correlation remains moderate due to the rather strong and opposite influence of soil moisture (Table 4) and to the (positive or negative) correlation of some 3-OH FA with MAAT. The RDA analysis also shows that the compounds used for the calculation of the RAN₁₅ and RAN₁₇ indices (*anteiso* and *normal* C₁₅/C₁₇ homologues) are located in the pH sector, orthogonal to MAAT (Fig. 7b). This explains why there are no linear relations between these indices and MAAT in soils from the French Alps (Fig. 5b, c).

4.2.4. Influence of vegetation and soil type on 3-OH FA and brGDGT distribution

As discussed above, the influence of local edaphic parameters (i.e. grain size, soil moisture, pH) related to soil type and vegetation on both brGDGT and 3-OH FA distribution was shown to be higher than that of MAAT. This is further confirmed by the distribution of the samples in the RDAs (Fig. 7 a, b), with the samples being distributed according to their affiliation to certain types of soils or vegetation communities. The fact that samples are grouped in clusters may partly be due to the fact that some of them are geographically proximal. But some of the samples, spatially distant, are also clustered in the RDA, for example, according to soil types : samples 20 to 25 (calcosols, between 1,540 m and 1,940 m a.s.l), samples 5 to 7 and 17 to 19 (brunisol, between 1,920 m and 2,688 m a.s.l), or vegetation compositions : samples 1 to 10 which are alpine meadow (between 2,531 and 2,700 m a.s.l.) (Fig. 7, Table 1). The calcosols are distributed over the entire right-hand side of the two RDAs, as they are essentially differentiated based on their alkaline pH. The calcosols are also distributed along axis 2, driven by altitude and relative soil moisture. Thus, lowland calcosols appear in the bottom or upper right quadrants of the two RDAs respectively (Fig. 7a, b), whereas subgroups of high-altitude calcosols, reflecting mountainous and subalpine vegetation covers, can be observed at the bottom or upper right, respectively. This shows that calcosols can also be differentiated based on the plant cover patterns and altitude. In contrast with the calcosols, brunisols are distributed throughout the whole correlation circle. However, they can be subdivided into 3 distinct subgroups based on the vegetation cover and altitude: a first subgroup with intermediate altitude

samples and mountainous vegetation, positively correlated with soil moisture; a second subgroup, with high altitude samples and meadow vegetation, negatively correlated with MAAT; a third subgroup of individuals, characterized by low altitude soils and lowland vegetation, positively correlated with MAAT. Altogether, the RDA results show that soil groups are discriminated according to their bacterial lipid distributions, which are strongly dependent on vegetation cover and soil types.

4.3. Development of local calibrations between the relative abundance of bacterial lipids and MAAT/pH

The wide diversity of microenvironments encountered the French Alps could explain the absence or weakness of the relationships between MAAT and brGDGT-/3-OH FA-based indices, as well as between pH and RIAN index. This stresses the need for identifying the individual lipids whose fractional abundance is mainly correlated with MAAT or pH, which is possible through RDA analyses (Fig. 7). The identification of these individual lipids then allow the development of local relationships between environmental parameters (MAAT/pH) and the relative abundances (%) of the selected compounds (Figs. 8 and 9), as detailed below.

4.3.1. *BrGDGTs*

Even though the MBT'_{5Me} index is not suitable for MAAT reconstruction in the French Alps ($R^2 = 0.35$; Fig. 5), the RDA analysis showed that the fractional abundance of some of the brGDGTs (mainly compound *IIIa* and to a lesser extent compounds *Iib'* and *Ib*) are moderately to strongly correlated with MAAT. An alternate transfer function with MAAT was defined based on a linear combination of the fractional abundance of these three compounds (Eq. 6; Fig.8):

$$\text{MAAT} = -0.255 \times [\text{IIIa}] + 0.195 \times [\text{Ib}] + 0.171 \times [\text{Iib}'] + 6.34 \quad (6)$$

$$(n = 49; R^2 = 0.69; \text{RMSE} = 2.26 \text{ } ^\circ\text{C})$$

This new calibration (Eq. 6; Fig. 8) shows a much higher determination coefficient and lower RMSE than the MBT'_{5Me}-MAAT relationship (Fig. 5a). The same approach was used to propose a new local calibration for the brGDGTs to reconstruct pH values, but this did not improve the linear relationship demonstrated between the CBT index and pH (Fig. 4a).

Altogether, these results suggest that brGDGTs can be used for both pH and temperature reconstructions even in highly diverse and contrasted environments such as the French Alps. Nevertheless, the present study shows that a detailed investigation of the environmental controls of brGDGT distribution and the development of local calibrations may be required to confidently use these compounds as paleoproxies.

4.3.2. 3-OH FAs

The RDA results allowed the identification of the individual 3-OH FAs whose relative abundance is mainly correlated with MAAT or pH (Fig. 7a). Two alternate transfer functions were proposed based on a linear combination of the relative abundance of 3-OH FAs (Eqs. 7 and 8), using a similar approach as for brGDGTs (Eq. 6):

$$\text{pH} = -0.144 \times [nC_{12}] + 0.177 \times [iC_{13}] - 0.171 \times [nC_{14}] + 0.148 \times [iC_{16}] + 10.01$$

$$(n = 49; R^2 = 0.70; \text{RMSE} = 0.6) \quad (7)$$

$$\text{MAAT} = -0.629 \times [nC_{10}] + 0.883 \times [iC_{15}] + 0.496 \times [iC_{17}] + 0.629 \times [nC_{18}] - 13.16$$

$$(n = 49; R^2 = 0.63; \text{RMSE} = 2.43 \text{ } ^\circ\text{C}) \quad (8)$$

The proposed relationship between pH and 3-OH FA relative abundances (Eq. 7; Fig 9a) presents a higher determination coefficient ($R^2 = 0.70$ vs. 0.43) and accuracy ($\text{RMSE} = 0.60$ vs. 0.83) than the one with the RIAN index. Similarly, the identification of the individual 3-OH FAs strongly influenced by MAAT allowed obtaining a new relationship with MAAT (Eq. 8; Fig. 9b) which was not visible through the previously defined RAN_{15} and RAN_{17} indices. This shows once again the interest and importance of constraining the environmental factors affecting the relative abundance of microbial lipids in complex and highly variable environments such as the French Alps, where conventional indices are not reliable for temperature and pH reconstructions. Specific calibrations have to be developed instead to take into account the effect of local confounding parameters on lipid relative distribution.

4.4. Constraints on the applicability of brGDGTs and 3-OH FAs as environmental proxies

3-OH FAs were proposed only recently as potential temperature and pH proxies in soils and were to date investigated in a limited amount of samples – ca. 70 soils, excluding the presently studied ones (Wang et al., 2016; Huguet et al., 2019). This contrasts with brGDGTs, whose applicability as environmental proxies in terrestrial (and aquatic) environments has been extensively investigated over the last 15 years (e.g. Weijers et al., 2007; Peterse et al., 2012; Coffinet et al., 2014; De Jonge et al., 2014; Huguet et al., 2014; Dang et al., 2016; Lei et al., 2016; Naafs et al., 2017; Dearing Crampton-Flood et al., 2020). Studies investigating the constraints on the applicability of 3-OH FAs as environmental proxies in terrestrial settings are thus needed. pH was shown to be the main factor influencing both brGDGT and 3-OH FA distribution in soils of the French Alps, even though RIAN shows a much more moderate correlation with a lower prediction interval (Fig. 4b; $R^2=0.43$, RMSE = 0.83) than CBT (Fig. 4a; $R^2 = 0.85$, RMSE = 0.42). The calibration between the linear combination of 3-OH FA relative abundances and pH proposed in this study (Eq. 7; Fig. 9a) is also slightly weaker ($R^2 = 0.70$) and less accurate (RMSE = 0.60) than the one with the CBT (Fig. 4a). Altogether, these results show the higher reliability of the latter index as a pH proxy in the French Alps. In contrast with pH, the MAAT was only moderately influencing the bacterial lipid distribution in soils reflected by the weak relationship between MBT'_{5Me} and MAAT and the absence of relationship of RAN₁₅ and RAN₁₇ with MAAT (Fig. 5). Nevertheless, the environmental variables investigated in the present study (including MAAT and pH) were not able to explain the total variability of the lipid distribution, the unexplained variation remaining higher for 3-OH FAs than for brGDGTs (Table 3). Seasonality might be one of the factors influencing the production of bacterial lipids in the French Alps soils, as previously suggested for brGDGTs in the French Jura Mountains (Huguet et al., 2013). Indeed, during part of the year, some of the French Alps soils are covered with snow, protecting them from extreme temperatures. Parameters such as microtopography or snowfall are known to have an important role on the thermal regime of soils and thus on the microorganisms living in them (Margesin et al., 2008). The effect of the thermal regime could therefore explain part of the dispersion remaining in the local calibrations between MAAT and bacteria lipid distribution.

The lack of information regarding the ecology of the 3-OH FA and brGDGT producers should indeed be taken into account while discussing the high uncertainty related to the lipid-based transfer functions. C₁₀ to C₁₈ 3-OH FAs, used for the calculation of the RAN₁₅ and RAN₁₇

pH/temperature proxies, are known to be produced by Gram-negative bacteria, which are a highly diverse group of microorganisms represented by numerous genera. This non-monophyletic group of bacteria does not share a common ancestor (Lecointre and Guyader, 2006), which explains the large genetic and biochemical differences between the various Gram-negative bacteria. The numerous genera and subgenera of Gram-negative bacteria are also characterized by highly diverse lipid profiles, with different relative abundances of 3-OH FAs, and with the whole suite of C₁₀-C₁₈ 3-OH FAs homologues not being present in all the strains (Wilkinson et al., 1988). Therefore, the 3-OH FA lipid distribution is highly dependent upon what Gram-negative bacterial species are present (e.g. Parker et al., 1982; Bhat and Carlson, 1992; Zelles, 1999). Furthermore, the diversity of Gram-negative bacteria varies with altitude (Margesin et al., 2009; Siles and Margesin, 2016). Taken together, this may partly explain the lack of relationship or poor to moderate correlations observed between 3-OH FA indices (RAN_{15/17}, RIAN) and MAAT/soil pH (Figs. 4b, 5b, c). Additionally, it might also not be excluded that the various soil Gram-negative bacteria genera/subgenera respond differently to variations of environmental parameters. In brief, the 3-OH FA profile of the various Gram-negative bacteria species likely reflects the diversity of microenvironments present in the French Alps, which are subjected concomitantly to large variations in several environmental parameters (MAAT, soil pH, soil moisture, microtopography, vegetation cover, soil type etc...).

In contrast, although they appear to be ubiquitous, brGDGTs might be produced by a more restricted number of bacterial species than 3-OH FAs. Indeed, so far only soil *Acidobacteria* have been found to contain the building blocks of brGDGT biosynthesis and are thus considered as potential brGDGT sources (Sinninghe Damsté et al., 2018). If the diversity of brGDGT producers is indeed lower than that of 3-OH FA-producing microorganisms, it may explain the more homogenous response and lower scatter of the relationships between MAAT/pH and brGDGT-derived indices than those with 3-OH FA indices (Figs. 4 and 5). Such relationships may also be affected by the different physiological responses of brGDGT and 3-OH FA producers to environmental parameters. These hypotheses remain purely speculative, as to date the information on brGDGT source microorganisms remains limited. This calls for further studies assessing and comparing the influence of environmental parameters on brGDGT and 3-OH FA producing bacteria in terrestrial environments. Such work is essential to improve the reliability and accuracy of the complementary temperature and pH proxies based on the two lipid families.

5. Conclusions

This study thoroughly investigated the environmental factors controlling the distribution of brGDGTs and 3-OH FAs in soils collected along well-documented altitudinal transects in the French Alps. The influence of local parameters (pH and to a lesser extent soil moisture and grain size, related to vegetation and soil types) on brGDGT and 3-OH FA was more important than MAAT. This likely explains the absence or weak relationships between MAAT and brGDGT/3-OH FA-based indices and stresses the need for identifying the individual lipids whose fractional abundance is correlated with MAAT or pH. Such work at the molecular level led to the development of strong local calibrations between the individual lipids identified through statistical analyses and MAAT/pH. They can be applied to soils from the French Alps, representative of highly contrasted microenvironments. The present study highlights the importance of constraining the environmental factors affecting the distribution of 3-OH FAs and brGDGTs in terrestrial settings prior to any environmental reconstruction using these lipid biomarkers. Such an approach should be reproduced in other sites, where local factors would also strongly influence the bacterial lipid distribution. Local effects are expected to explain a large part of the scatter observed in the global calibrations between MAAT/pH and 3-OH FA as well as brGDGT distribution. These local confounding parameters may notably explain why the calibration between 3-OH FA indices ($RAN_{15/17}$) and MAAT in the French Alps differ from those previously obtained in other sites. As 3-OH FAs and brGDGTs may be produced by different microorganisms, further work is needed to assess and compare the impact of environmental parameters, especially temperature and pH, on the microbial diversity in contrasted soils and the associated lipid profiles. Even though the lack of knowledge on brGDGT-producing bacteria complicates such studies, the latter are essential to improve the reliability and accuracy of the complementary temperature and pH proxies based on 3-OH FAs and brGDGTs.

Acknowledgments. We thank Sorbonne Université for a PhD scholarship to P.V. and the Labex MATISSE (Sorbonne Université) for financial support. The EC2CO program (CNRS/INSU – BIOHEFECT/MICROBIEN) is thanked for funding to the SHAPE project. We thank A. Thibault for assisting in the development of new local calibrations. We are grateful to P. Choler for discussions on alpine vegetation and climate, and for comments on the manuscript. We thank two anonymous reviewers for their constructive comments.

References

- Anderson, V.J., Shanahan, T.M., Saylor, J.E., Horton, B.K., Mora, A.R., 2014. Sources of local and regional variability in the MBT'/CBT paleotemperature proxy: Insights from a modern elevation transect across the Eastern Cordillera of Colombia. *Organic Geochemistry* 69, 42–51.
- Bartlett, M.G., Chapman, D.S., Harris, R.N., 2006. A Decade of Ground–Air Temperature Tracking at Emigrant Pass Observatory, Utah. *Journal of Climate* 19, 3722–3731.
- Beales, N., 2004. Adaptation of Microorganisms to Cold Temperatures, Weak Acid Preservatives, Low pH, and Osmotic Stress: A Review. *Comprehensive Reviews in Food Science and Food Safety* 3, 1–20.
- Bhandari J., Zhang Y., 2019. Effect of altitude and soil properties on biomass and plant richness in the grasslands of Tibet, China, and Manang District, Nepal. *Ecosphere* 10, e02915.
- Bhat, U.R., Carlson, R.W., 1992. A new method for the analysis of amide-linked hydroxy fatty acids in lipid-As from gram-negative bacteria. *Glycobiology* 2, 535–539.
- Bounemoura, Z., Lambert, K., Cadel, G., Choler, P., Manneville, O., & Michalet, R. 1998. Influence des facteurs édapho-climatiques sur la distribution des pelouses alpines dans le massif du Galibier (Alpes Françaises). *ÉCOLOGIE-BRUNOY*, 29, 53-58.
- Braak, C.J.F. ter, Smilauer, P., 2002. CANOCO Reference Manual and CanoDraw for Windows User's Guide: Software for Canonical Community Ordination (version 4.5). www.canoco.com, Ithaca NY, USA.
- Carlson, B.Z., Corona, M.C., Dentant, C., Bonet, R., Thuiller, W., Choler, P., 2017. Observed long-term greening of alpine vegetation—a case study in the French Alps. *Environmental Research Letters* 12, 114006.
- Carter, M.R., Gregorich, E.G., Gregorich, E.G., 2007. *Soil Sampling and Methods of Analysis*. CRC Press. doi:10.1201/9781420005271
- Cheng, J.Y.W., Hui, E.L.C., Lau, A.P.S., 2012. Bioactive and total endotoxins in atmospheric aerosols in the Pearl River Delta region, China. *Atmospheric Environment* 47, 3–11.
- Cheng- Jim, J. I., Yang, Y.H., Han, W.X., He, Y.F., Smith, J., Smith, P., 2014. Climatic and edaphic controls on soil pH in alpine grasslands on the Tibetan Plateau, China: a quantitative analysis. *Pedosphere* 24, 39– 44.
- Choler, P., 2018. Winter soil temperature dependence of alpine plant distribution: Implications for anticipating vegetation changes under a warming climate. *Perspectives in Plant Ecology, Evolution and Systematics*, Special issue on Alpine and arctic plant communities : a worldwide perspective 30, 6–15.
- Ciesielski, H., Sterckeman, T., Santerne, M., Willery, J., 1997. Determination of cation exchange capacity and exchangeable cations in soils by means of cobalt hexamine trichloride. Effects of experimental conditions. *Agronomie* 17, 1–7.
- Coffinet, S., Huguet, A., Williamson, D., Fosse, C., Derenne, S., 2014. Potential of GDGTs as a temperature proxy along an altitudinal transect at Mount Rungwe (Tanzania). *Organic Geochemistry* 68, 82–89.
- Coffinet, S., Huguet, A., Bergonzini, L., Pedentchouk, N., Williamson, D., Anquetil, C., Gałka, M., Kołaczek, P., Karpińska-Kołaczek, M., Majule, A., Laggoun-Défarge, F., Wagner, T., Derenne, S., 2018. Impact of climate change on the ecology of the Kyambangunguru crater marsh in southwestern Tanzania during the Late Holocene. *Quaternary Science Reviews* 196, 100–117.
- Conant, R.T., Ryan, M.G., Ågren, G.I., Birge, H.E., Davidson, E.A., Eliasson, P.E., Evans, S.E., Frey, S.D., Giardina, C.P., Hopkins, F.M., Hyvönen, R., Kirschbaum, M.U.F., Lavallee, J.M., Leifeld, J., Parton, W.J., Steinweg, J.M., Wallenstein, M.D., Wetterstedt, J.Å.M., Bradford, M.A., 2011. Temperature and soil organic matter

- decomposition rates – synthesis of current knowledge and a way forward. *Global Change Biology* 17, 3392–3404.
- Crave, A., Gascuel- Odoux, C., 1997. The Influence of Topography on Time and Space Distribution of Soil Surface Water Content. *Hydrological Processes* 11, 203–210.
- Dang, X., Xue, J., Yang, H., Xie, S., 2016. Environmental impacts on the distribution of microbial tetraether lipids in Chinese lakes with contrasting pH: Implications for lacustrine paleoenvironmental reconstructions. *Science China Earth Sciences* 59, 939–950.
- Davidson, E.A., Belk, E., Boone, R.D., 1998. Soil water content and temperature as independent or confounded factors controlling soil respiration in a temperate mixed hardwood forest. *Global Change Biology* 4, 217–227.
- Davidson, E. A., Janssens, I.A., 2006. Temperature sensitivity of soil carbon decomposition and feedbacks to climate change. *Nature* 440, 165– 173.
- Davtian, N., Ménot, G., Bard, E., Poulenard, J., Podwojewski, P., 2016. Consideration of soil types for the calibration of molecular proxies for soil pH and temperature using global soil datasets and Vietnamese soil profiles. *Organic Geochemistry* 101, 140–153.
- De Jonge, C., Hopmans, E.C., Zell, C.I., Kim, J.-H., Schouten, S., Sinninghe Damsté, J.S., 2014. Occurrence and abundance of 6-methyl branched glycerol dialkyl glycerol tetraethers in soils: Implications for palaeoclimate reconstruction. *Geochimica et Cosmochimica Acta* 141, 97–112.
- De Jonge, C., Radujković, D., Sigurdsson, B.D., Weedon, J.T., Janssens, I., Peterse, F., 2019. Lipid biomarker temperature proxy responds to abrupt shift in the bacterial community composition in geothermally heated soils. *Organic Geochemistry* 137, 103897.
- Dearing Crampton-Flood, E., Tierney, J.E., Peterse, F., Kirkels, F.M.S.A., Sinninghe Damsté, J.S., 2020. BayMBT: A Bayesian calibration model for branched glycerol dialkyl glycerol tetraethers in soils and peats. *Geochimica et Cosmochimica Acta* 268, 142–159.
- Denich, T.J., Beaudette, L.A., Lee, H., Trevors, J.T., 2003. Effect of selected environmental and physico-chemical factors on bacterial cytoplasmic membranes. *Journal of Microbiological Methods* 52, 149–182.
- Ding, S., Xu, Y., Wang, Y., He, Y., Hou, J., Chen, L., He, J.-S., 2015. Distribution of branched glycerol dialkyl glycerol tetraethers in surface soils of the Qinghai–Tibetan Plateau: implications of brGDGTs-based proxies in cold and dry regions. *Biogeosciences* 12, 3141–3151.
- Dirghangi, S.S., Pagani, M., Hren, M.T., Tipple, B.J., 2013. Distribution of glycerol dialkyl glycerol tetraethers in soils from two environmental transects in the USA. *Organic Geochemistry* 59, 49–60.
- Djukic, I., Zehetner, F., Tatzber, M., Gerzabek, M.H., 2010. Soil organic-matter stocks and characteristics along an Alpine elevation gradient. *Journal of Plant Nutrition and Soil Science* 173, 30–38.
- Du, B., Liu, C., Kang, H., Zhu, P., Yin, S., Shen, G., Hou, J., Ilvesniemi, H., 2014. Climatic control on plant and soil $\delta^{13}\text{C}$ along an altitudinal transect of Lushan Mountain in subtropical China: Characteristics and interpretation of soil carbon dynamics. *PLOS One*, <https://doi.org/10.1371/journal.pone.0086440>.
- Durand, Y., Laternser, M., Giraud, G., Etchevers, P., Lesaffre, B., & Mérindol, L. 2009. Reanalysis of 875 44 yr of climate in the French Alps (1958–2002): methodology, model validation, climatology, 876 and trends for air temperature and precipitation. *Journal of Applied Meteorology and 877 Climatology*, 48(3), 429–449.
- Eglinton, T.I., Eglinton, G., 2008. Molecular proxies for paleoclimatology. *Earth and Planetary Science Letters* 275, 1–16.

- Ernst, R., Ejlsing, C.S., Antonny, B., 2016. Homeoviscous Adaptation and the Regulation of Membrane Lipids. *Journal of Molecular Biology, Molecular Biology of Membrane Lipids* 428, 4776–4791.
- Fierer, N., Jackson, R.B., 2006. The diversity and biogeography of soil bacterial communities. *Proceedings of the National Academy of Sciences* 103, 626–631.
- Gómez-Plaza, A., Martínez-Mena, M., Albaladejo, J., Castillo, V.M., 2001. Factors regulating spatial distribution of soil water content in small semiarid catchments. *Journal of Hydrology* 253, 211–226.
- Gutiérrez-Girón, A., Díaz-Pinés, E., Rubio, A., Gavilán, R.G., 2015. Both altitude and vegetation affect temperature sensitivity of soil organic matter decomposition in Mediterranean high mountain soils. *Geoderma* 237–238, 1–8.
- Hazel, J.R., Eugene Williams, E., 1990. The role of alterations in membrane lipid composition in enabling physiological adaptation of organisms to their physical environment. *Progress in Lipid Research* 29, 167–227.
- Hemkemeyer, M., Dohrmann, A.B., Christensen, B.T., Tebbe, C.C., 2018. Bacterial Preferences for Specific Soil Particle Size Fractions Revealed by Community Analyses. *Frontiers in Microbiology* 9. doi:10.3389/fmicb.2018.00149
- Hofmann, K., Lamprecht, A., Pauli, H., Illmer, P., 2016. Distribution of Prokaryotic Abundance and Microbial Nutrient Cycling Across a High-Alpine Altitudinal Gradient in the Austrian Central Alps is Affected by Vegetation, Temperature, and Soil Nutrients. *Microbial Ecology* 72, 704–716.
- Hopmans, E.C., Schouten, S., Sinninghe Damsté, J.S., 2016. The effect of improved chromatography on GDGT-based palaeoproxies. *Organic Geochemistry* 93, 1–6.
- Huguet, A., Fosse, C., Laggoun-Défarge, F., Toussaint, M.-L., Derenne, S., 2010. Occurrence and distribution of glycerol dialkyl glycerol tetraethers in a French peat bog. *Organic Geochemistry* 41, 559–572.
- Huguet, A., Fosse, C., Laggoun-Défarge, F., Delarue, F., Derenne, S., 2013. Effects of a short-term experimental microclimate warming on the abundance and distribution of branched GDGTs in a French peatland. *Geochimica et Cosmochimica Acta* 105, 294–315.
- Huguet, A., Francez, A.-J., Jusselme, M.D., Fosse, C., Derenne, S., 2014. A climatic chamber experiment to test the short term effect of increasing temperature on branched GDGT distribution in Sphagnum peat. *Organic Geochemistry* 73, 109–112.
- Huguet, A., Coffinet, S., Roussel, A., Gayraud, F., Anquetil, C., Bergonzini, L., Bonanomi, G., Williamson, D., Majule, A., Derenne, S., 2019. Evaluation of 3-hydroxy fatty acids as a pH and temperature proxy in soils from temperate and tropical altitudinal gradients. *Organic Geochemistry* 129, 1–13.
- Huguet, C., Hopmans, E.C., Febo-Ayala, W., Thompson, D.H., Sinninghe Damsté, J.S., Schouten, S., 2006. An improved method to determine the absolute abundance of glycerol dibiphytanyl glycerol tetraether lipids. *Organic Geochemistry* 37, 1036–1041.
- Idso, S.B., Schmugge, T.J., Jackson, R.D., Reginato, R.J., 1975. The utility of surface temperature measurements for the remote sensing of surface soil water status. *Journal of Geophysical Research* (1896-1977) 80, 3044–3049.
- Keinänen, M.M., Korhonen, L.K., Martikainen, P.J., Vartiainen, T., Miettinen, I.T., Lehtola, M.J., Nenonen, K., Pajunen, H., Kontro, M.H., 2003. Gas chromatographic–mass spectrometric detection of 2- and 3-hydroxy fatty acids as methyl esters from soil, sediment and biofilm. *Journal of Chromatography B* 783, 443–451.
- Lecointre G. and Guyader H. L. 2006. *The Tree of Life: A Phylogenetic Classification.*, Harvard University Press

- 957 Lee, A.K.Y., Chan, C.K., Fang, M., Lau, A.P.S., 2004. The 3-hydroxy fatty acids as biomarkers
958 for quantification and characterization of endotoxins and Gram-negative bacteria in
959 atmospheric aerosols in Hong Kong. *Atmospheric Environment* 38, 6307–6317.
- 960 Lei, Y., Yang, H., Dang, X., Zhao, S., Xie, S., 2016. Absence of a significant bias towards
961 summer temperature in branched tetraether-based paleothermometer at two soil sites
962 with contrasting temperature seasonality. *Organic Geochemistry* 94, 83–94.
- 963 Lepage, C., Fayolle, F., Hermann, M., Vandecasteele, J.P., 1987. Changes in Membrane Lipid
964 Composition of *Clostridium acetobutylicum* during Acetone-Butanol Fermentation:
965 Effects of Solvents, Growth Temperature and pH. *Microbiology*, 133, 103–110.
- 966 Liang, J., Russell, J.M., Xie, H., Lupien, R.L., Si, G., Wang, J., Hou, J., Zhang, G., 2019.
967 Vegetation effects on temperature calibrations of branched glycerol dialkyl glycerol
968 tetraether (brGDGTs) in soils. *Organic Geochemistry* 127, 1–11.
- 969 Liu, W., Wang, H., Zhang, C.L., Liu, Z., He, Y., 2013. Distribution of glycerol dialkyl glycerol
970 tetraether lipids along an altitudinal transect on Mt. Xiangpi, NE Qinghai-Tibetan
971 Plateau, China. *Organic Geochemistry* 57, 76–83.
- 972 Loomis, S.E., Russell, J.M., Ladd, B., Street-Perrott, F.A., Sinninghe Damsté, J.S., 2012.
973 Calibration and application of the branched GDGT temperature proxy on East African
974 lake sediments. *Earth and Planetary Science Letters* 357–358, 277–288.
- 975 Margesin, R., Jud, M., Tscherko, D., Schinner, F., 2009. Microbial communities and activities
976 in alpine and subalpine soils: Communities and activities in alpine and subalpine soils.
977 *FEMS Microbiology Ecology* 67, 208–218.
- 978 Menges, J., Huguet, C., Alcañiz, J.M., Fietz, S., Sachse, D., Rosell-Melé, A., 2014. Influence
979 of water availability in the distributions of branched glycerol dialkyl glycerol tetraether
980 in soils of the Iberian Peninsula. *Biogeosciences* 11, 2571–2581.
- 981 Metson, A.J., 1957. Methods of Chemical Analysis for Soil Survey Samples. *Soil Science* 83,
982 245.
- 983 Mueller-Niggemann, C., Utami, S.R., Marxen, A., Mangelsdorf, K., Bauersachs, T., Schwark,
984 L., 2016. Distribution of tetraether lipids in agricultural soils – differentiation
985 between paddy and upland management. *Biogeosciences* 13, 1647–1666.
- 986 Naafs, B.D.A., Gallego-Sala, A.V., Inglis, G.N., Pancost, R.D., 2017. Refining the global
987 branched glycerol dialkyl glycerol tetraether (brGDGT) soil temperature calibration.
988 *Organic Geochemistry* 106, 48–56.
- 989 Naeher, S., Peterse, F., Smittenberg, R.H., Niemann, H., Zigah, P.K., Schubert, C.J., 2014.
990 Sources of glycerol dialkyl glycerol tetraethers (GDGTs) in catchment soils, water
991 column and sediments of Lake Rotsee (Switzerland) – Implications for the application
992 of GDGT-based proxies for lakes. *Organic Geochemistry* 66, 164–173.
- 993 Peterse, F., van der Meer, J., Schouten, S., Weijers, J.W.H., Fierer, N., Jackson, R.B., Kim, J.-
994 H., Sinninghe Damsté, J.S., 2012. Revised calibration of the MBT–CBT
995 paleotemperature proxy based on branched tetraether membrane lipids in surface soils.
996 *Geochimica et Cosmochimica Acta* 96, 215–229.
- 997 Parker, J.H., Smith, G.A., Fredrickson, H.L., Vestal, J.R., White, D.C., 1982. Sensitive assay,
998 based on 959 hydroxy fatty acids from lipopolysaccharide lipid A, from Gram negative
999 bacteria in sediments. *Applied and Environmental Microbiology* 44.
- 1000 Peterse, F., Moy, C.M., Eglinton, T.I., 2015. A laboratory experiment on the behaviour of soil-
1001 derived core and intact polar GDGTs in aquatic environments. *Biogeosciences* 12, 933–
1002 943.
- 1003 Peterse, F., Eglinton, T.I., 2017. Grain Size Associations of Branched Tetraether Lipids in Soils
1004 and Riverbank Sediments: Influence of Hydrodynamic Sorting Processes. *Frontiers in*
1005 *Earth Science* 5. doi:10.3389/feart.2017.00049

- Powers, L., Werne, J.P., Vanderwoude, A.J., Sinninghe Damsté, J.S., Hopmans, E.C., Schouten, S., 2010. Applicability and calibration of the TEX86 paleothermometer in lakes. *Organic Geochemistry* 41, 404–413.
- R Core Team, 2014. R: A language and environment for statistical computing. R Foundation for Statistical Computing, Vienna, Austria.
- Russell, N.J., 1989. Adaptive modifications in membranes of halotolerant and halophilic microorganisms. *Journal of Bioenergetics and Biomembranes* 21, 93–113.
- Russell, N.J., Evans, R.I., ter Steeg, P.F., Hellemons, J., Verheul, A., Abee, T., 1995. Membranes as a target for stress adaptation. *International Journal of Food Microbiology, Physiology of Food Poisoning Microorganisms, AAIR Concerted Action PL920630* 28, 255–261.
- Saraf, A., Larsson, L., Burge, H., Milton, D., 1997. Quantification of ergosterol and 3-hydroxy fatty acids in settled house dust by gas chromatography-mass spectrometry: comparison with fungal culture and determination of endotoxin by a *Limulus* amoebocyte lysate assay. *Applied and Environmental Microbiology* 63, 2554–2559.
- Schouten, S., Hopmans, E.C., Schefuß, E., Sinninghe Damsté, J.S., 2002. Distributional variations in marine crenarchaeotal membrane lipids: a new tool for reconstructing ancient sea water temperatures? *Earth and Planetary Science Letters* 204, 265–274.
- Schouten, S., Rijpstra, W.I.C., Durisch-Kaiser, E., Schubert, C.J., Sinninghe Damsté, J.S., 2012. Distribution of glycerol dialkyl glycerol tetraether lipids in the water column of Lake Tanganyika. *Organic Geochemistry, Advances in Organic Geochemistry 2011: Proceedings of the 25th International Meeting on Organic Geochemistry* 53, 34–37.
- Schouten, S., Hopmans, E.C., Sinninghe Damsté, J.S., 2013. The organic geochemistry of glycerol dialkyl glycerol tetraether lipids: A review. *Organic Geochemistry* 54, 19–61.
- Shen, C., Shi, Y., Fan, K., He, J.-S., Adams, J.M., Ge, Y., Chu, H., 2019. Soil pH dominates elevational diversity pattern for bacteria in high elevation alkaline soils on the Tibetan Plateau. *FEMS Microbiology Ecology* 95. doi:10.1093/femsec/fiz003
- Siles, J.A., Margesin, R., 2016. Abundance and Diversity of Bacterial, Archaeal, and Fungal Communities Along an Altitudinal Gradient in Alpine Forest Soils: What Are the Driving Factors? *Microbial Ecology* 72, 207–220.
- Sinensky, M., 1974. Homeoviscous Adaptation—A Homeostatic Process that Regulates the Viscosity of Membrane Lipids in *Escherichia coli*. *Proceedings of the National Academy of Sciences* 71, 522–525.
- Singer, S.J., Nicolson, G.L., 1972. The Fluid Mosaic Model of the Structure of Cell Membranes. *Science* 175, 720–731.
- Sinninghe Damsté, J.S., Hopmans, E.C., Pancost, R.D., Schouten, S., Geenevasen, J.A.J., 2000. Newly discovered non-isoprenoid glycerol dialkylglycerol tetraether lipids in sediments. *Chemical Communications* 1683–1684.
- Sinninghe Damsté, J.S., Ossebaar, J., Schouten, S., Verschuren, D., 2008. Altitudinal shifts in the branched tetraether lipid distribution in soil from Mt. Kilimanjaro (Tanzania): Implications for the MBT/CBT continental palaeothermometer. *Organic Geochemistry, Advances in Organic Geochemistry 2007* 39, 1072–1076.
- Sinninghe Damsté, J.S., Rijpstra, W.I.C., Hopmans, E.C., Weijers, J.W.H., Foesel, B.U., Overmann, J., Dedysh, S.N., 2011. 13,16-Dimethyl Octacosanedioic Acid (iso-Diabolic Acid), a Common Membrane-Spanning Lipid of Acidobacteria Subdivisions 1 and 3. *Appl. Environ. Microbiol.* 77, 4147–4154.
- Sinninghe Damsté, J.S., W.I.C., Hopmans, E.C., Foesel, B.U., Wüst, P.K., Overmann, J., Tank, M., Bryant, D.A., Dunfield, P.F., Houghton, K., Stott, M.B., 2014. Ether- and Ester-Bound iso-Diabolic Acid and Other Lipids in Members of Acidobacteria Subdivision 4. *Appl. Environ. Microbiol.* 80, 5207–5218.

- Sinninghe Damsté, J.S., Rijpstra, W.I.C., Foesel, B.U., Huber, K.J., Overmann, J., Nakagawa, S., Kim, J.J., Dunfield, P.F., Dedysh, S.N., Villanueva, L., 2018. An overview of the occurrence of ether- and ester-linked iso-diabolic acid membrane lipids in microbial cultures of the Acidobacteria: Implications for brGDGT paleoproxies for temperature and pH. *Organic Geochemistry* 124, 63–76.
- Smith, J.L., Halvorson, J.J., Bolton, H., 2002. Soil properties and microbial activity across a 500m elevation gradient in a semi-arid environment. *Soil Biology and Biochemistry* 34, 1749–1757.
- Szponar, B., Norin, E., Midtvedt, T., Larsson, L., 2002. Limitations in the use of 3-hydroxy fatty acid analysis to determine endotoxin in mammalian samples. *Journal of Microbiological Methods* 50, 283–289.
- Szponar, B., Kraśnik, L., Hryniewiecki, T., Gamian, A., Larsson, L., 2003. Distribution of 3-Hydroxy Fatty Acids in Tissues after Intraperitoneal Injection of Endotoxin. *Clinical Chemistry* 49, 1149–1153.
- Vionnet, V., Brun, E., Morin, S., Boone, A., Faroux, S., Le Moigne, P., ... & Willemet, J. M. (2012). 1031 The detailed snowpack scheme Crocus and its implementation in SURFEX v7. 2.
- Wakeham, S.G., Pease, T.K., Benner, R., 2003. Hydroxy fatty acids in marine dissolved organic matter as indicators of bacterial membrane material. *Organic Geochemistry* 34, 857–868.
- Wang, C., Bendle, J., Yang, Y., Yang, H., Sun, H., Huang, J., Xie, S., 2016. Impacts of pH and temperature on soil bacterial 3-hydroxy fatty acids: Development of novel terrestrial proxies. *Organic Geochemistry* 94, 21–31.
- Wang, C., Bendle, J.A., Zhang, H., Yang, Y., Liu, D., Huang, J., Cui, J., Xie, S., 2018. Holocene temperature and hydrological changes reconstructed by bacterial 3-hydroxy fatty acids in a stalagmite from central China. *Quaternary Science Reviews* 192, 97–105.
- Wang, M., Zheng, Z., Man, M., Hu, J., Gao, Q., 2017. Branched GDGT-based paleotemperature reconstruction of the last 30,000 years in humid monsoon region of Southeast China. *Chemical Geology* 463, 94–102.
- Watanabe, Y., Takakuwa, M., 1984. Effect of Sodium Chloride on Lipid Composition of *Saccharomyces rouxii*. *Agricultural and Biological Chemistry* 48, 2415–2422.
- Weber, Y., De Jonge, C., Rijpstra, W.I.C., Hopmans, E.C., Stadnitskaia, A., Schubert, C.J., Lehmann, M.F., Sinninghe Damsté, J.S., Niemann, H., 2015. Identification and carbon isotope composition of a novel branched GDGT isomer in lake sediments: Evidence for lacustrine branched GDGT production. *Geochimica et Cosmochimica Acta* 154, 118–129.
- Wei, K., Jia, G., 2009. Soil n-alkane $\delta^{13}\text{C}$ along a mountain slope as an integrator of altitude effect on plant species $\delta^{13}\text{C}$. *Geophysical Research Letters* 36, L11401.
- Weijers, J.W.H., Schouten, S., Spaargaren, O.C., Sinninghe Damsté, J.S., 2006. Occurrence and distribution of tetraether membrane lipids in soils: Implications for the use of the TEX86 proxy and the BIT index. *Organic Geochemistry, Advances in Organic Geochemistry* 2005 37, 1680–1693.
- Weijers, J.W.H., Schouten, S., van den Donker, J.C., Hopmans, E.C., Sinninghe Damsté, J.S., 2007. Environmental controls on bacterial tetraether membrane lipid distribution in soils. *Geochimica et Cosmochimica Acta* 71, 703–713.
- Weijers, J.W.H., Bernhardt, B., Peterse, F., Werne, J.P., Dungait, J.A.J., Schouten, S., Sinninghe Damsté, J.S., 2011. Absence of seasonal patterns in MBT–CBT indices in mid-latitude soils. *Geochimica et Cosmochimica Acta* 75, 3179–3190.

1104 Weijers, Johan W. H., Steinmann, P., Hopmans, E.C., Schouten, S., Sinninghe Damsté, J.S.,
1105 2011. Bacterial tetraether membrane lipids in peat and coal: Testing the MBT–CBT
1106 temperature proxy for climate reconstruction. *Organic Geochemistry* 42, 477–486.
1107 Wilkinson, S.G. 1988 Gram-negative bacteria. In: Ratledge C., Wilkinson S.G. (Eds),
1108 *Microbial Lipids*, 1063 vol. 1. Academic Press, New York, pp. 199-488.
1109 Wollenweber, H.W., Rietschel, E.T., 1990. Analysis of lipopolysaccharide (lipid A) fatty acids.
1110 *Journal of Microbiological Methods* 11, 195–211.
1111 Yang, Y., Wang, C., Bendle, J.A., Yu, X., Gao, C., Lü, X., Ruan, X., Wang, R., Xie, S., 2020.
1112 A new sea surface temperature proxy based on bacterial 3-hydroxy fatty acids. *Organic*
1113 *Geochemistry* 141, 103975.
1114 Zell, C., Kim, J.-H., Balsinha, M., Dorhout, D., Fernandes, C., Baas, M., Sinninghe Damsté,
1115 J.S., 2014. Transport of branched tetraether lipids from the Tagus River basin to the
1116 coastal ocean of the Portuguese margin: consequences for the interpretation of the
1117 MBT'/CBT paleothermometer. *Biogeosciences* 11, 5637–5655.
1118 Zelles, L., Bai, Q.Y., Rackwitz, R., Chadwick, D., Beese, F., 1995. Determination of
1119 phospholipid- and lipopolysaccharide-derived fatty acids as an estimate of microbial
1120 biomass and community structures in soils. *Biology and Fertility of Soils* 19, 115–123.
1121 Zelles, L., 1999. Fatty acid patterns of phospholipids and lipopolysaccharides in the
1122 characterisation of microbial communities in soil: a review. *Biology and Fertility of*
1123 *Soils* 29, 111–129.
1124

Figure and table captions

Figure 1. Location of the two massifs of the French Alps investigated in this study. Images Google Satellites. Exact sampling locations is shown in Supp. Figure 1.

Figure 2. Altitudinal transect between the Bauges and Lautaret-Galibier massifs showing the dominant plant species and the different alpine stages.

Figure 3. Average distribution of (a) brGDGTs and (b) 3-OH FAs in the 49 soil samples of the French Alps.

Figure 4. (a) Linear regression between CBT and pH along the two massifs in the French Alps. The black dotted line corresponds to the global linear regression between CBT and pH from De Jonge et al. (2014). (b) Linear regression between RIAN and pH along the two massifs in the French Alps. The black dotted line corresponds to the linear regression between RIAN and pH from Huguet et al. (2019). Dotted and colored lines represent the 95% prediction interval for each regression and colored areas represent the 95% confidence interval for each regression.

Figure 5. (a) Linear regression between MAAT and MBT'_{5Me} along the two massifs in the French Alps. The black dotted line corresponds to global the linear regression between MBT'_{5Me} and MAAT from De Jonge et al. (2014). Linear regressions between (b) RAN₁₅ and (c) RAN₁₇ along the two massifs in the French Alps. Dotted and colored lines represent the 95% prediction interval for each linear regression and colored areas represent the 95% confidence interval for each regression.

Figure 6. Correlation matrix between the different environmental variables and soil properties. Correlation coefficients in red (negative correlation) or blue (positive correlation) are statistically significant. Red variables have been chosen as explanatory variables for statistical tests.

Figure 7. Triplot presenting the results of the RDA carried out on the relative abundances of (a) brGDGTs and (b) 3-OH FAs and the non-redundant physicochemical parameters: pH, MAAT, soil moisture, sand and clay contents.

Figure 8. MAAT estimated using the new calibration based on a linear combination of brGDGT relative abundances (Eq. 6) vs. MAAT observed along the the Bauges and Lautaret-Galibier massifs. The roman numerals correspond to the different GDGT structures presented in De Jonge et al. (2014).

Figure 9. (a) pH estimated using the new calibration based on a linear combination of 3-OH FA relative abundances (Eq. 7) vs. pH observed along the Bauges and Lautaret-Galibier massifs. (b) MAAT estimated using the new calibration based on a linear combination of 3-OH relative abundances (Eq. 8) vs. MAAT observed along the Bauges and Lautaret-Galibier massifs. The roman numerals correspond to the different GDGT structures presented in De Jonge et al. (2014).

Table 1. List of the soil samples associated with corresponding soil type and vegetation collected along the Bauges and Lautaret-Galibier massifs.

Table 2. Physicochemical characteristics of the 49 samples collected along the Bauges and Lautaret-Galibier massifs. The numbering of the samples corresponds to that used in Table 1. Samples with stars represent sites instrumented with temperature sensors.

Table 3. RDA correlation coefficients of the environmental variables selected along axes 1 and 2.

Table 4. Quantification of the influence of the different environmental variables on brGDGTs and 3-OH FAs. Statistical significancies are shown as follows: *** ($0 < p < 0.001$); ** ($0.001 < p < 0.01$); * ($0.01 < p < 0.05$); ° ($0.05 < p < 0.1$).

Supplementary Figure 1. Location of the sampling sites along the a) Bauges and b) Lautaret-Galibier massifs.

Supplementary Figure 2. Linear model used to reconstruct MAAT along the Bauges and Lautaret-Galibier massifs. Dotted lines represent the 95% prediction interval for the linear regression and colored area represent the 95% confidence interval.

Supplementary Table 1. Relative abundances (%) of the *normal*, *iso* and *anteiso* 3-OH FAs in soils from the French Alps and corresponding indices.

Supplementary Table 2. Relative abundances (%) of the brGDGTs in soils from the French Alps and corresponding indices.

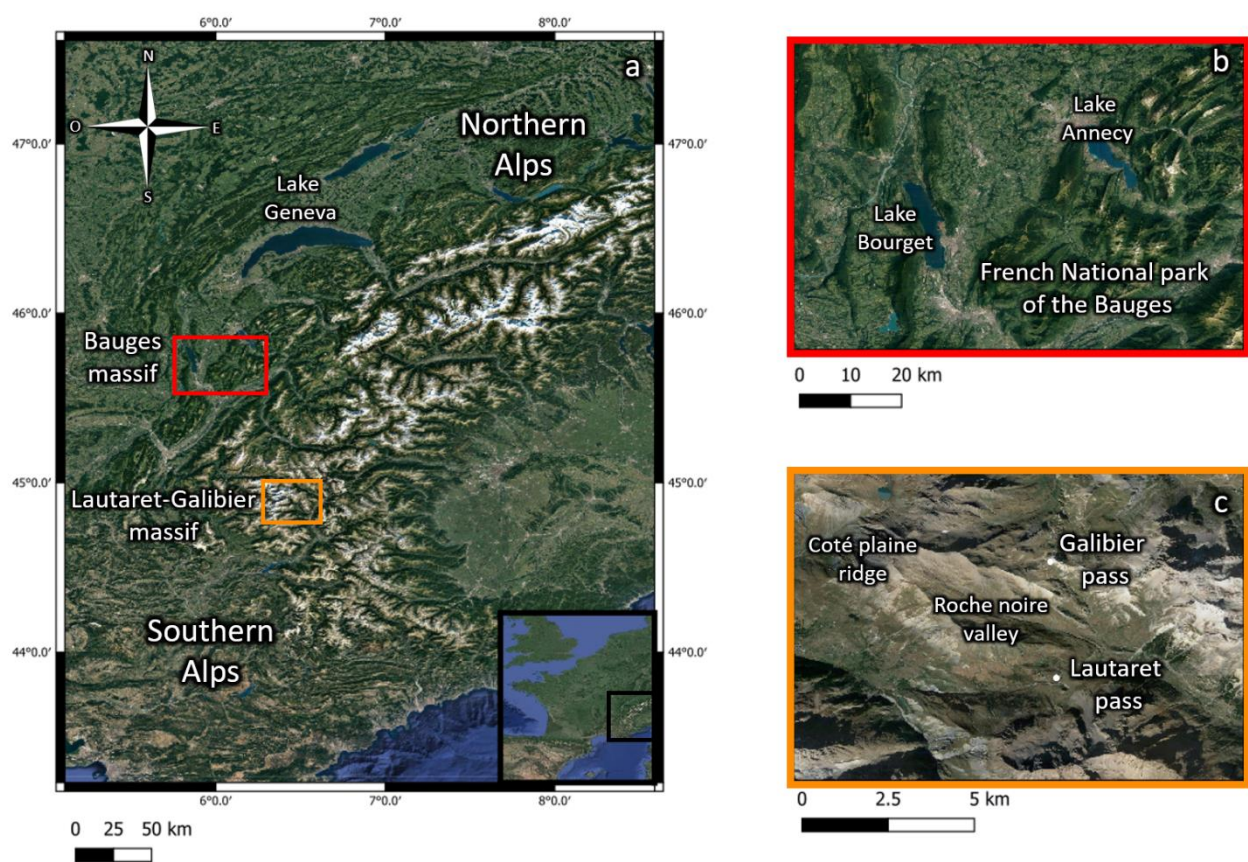


Figure 1

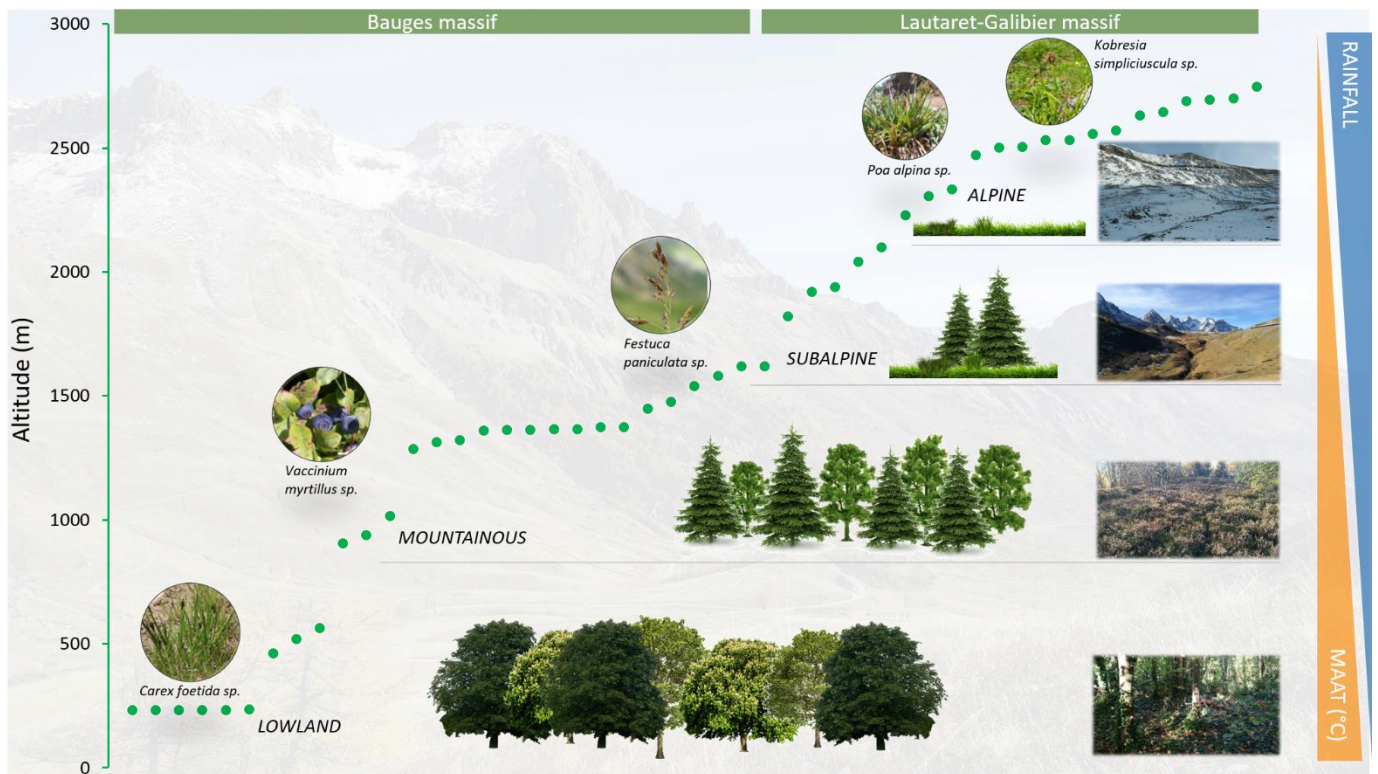


Figure 2

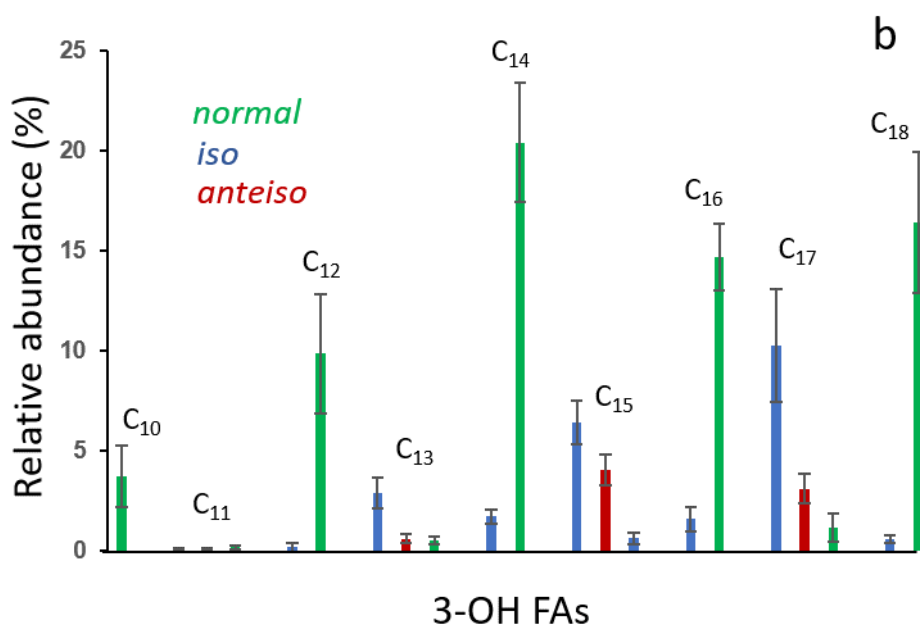
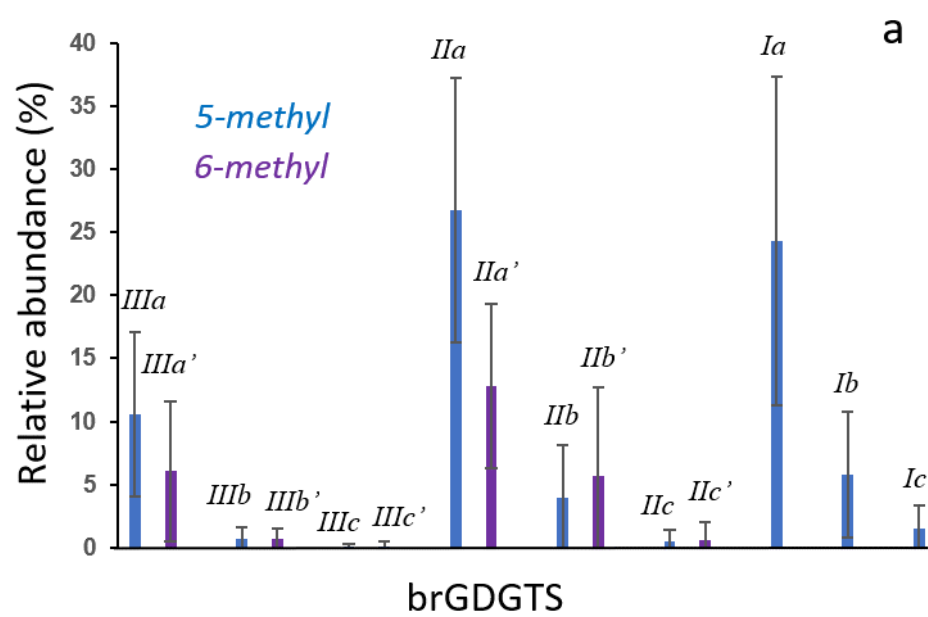


Figure 3

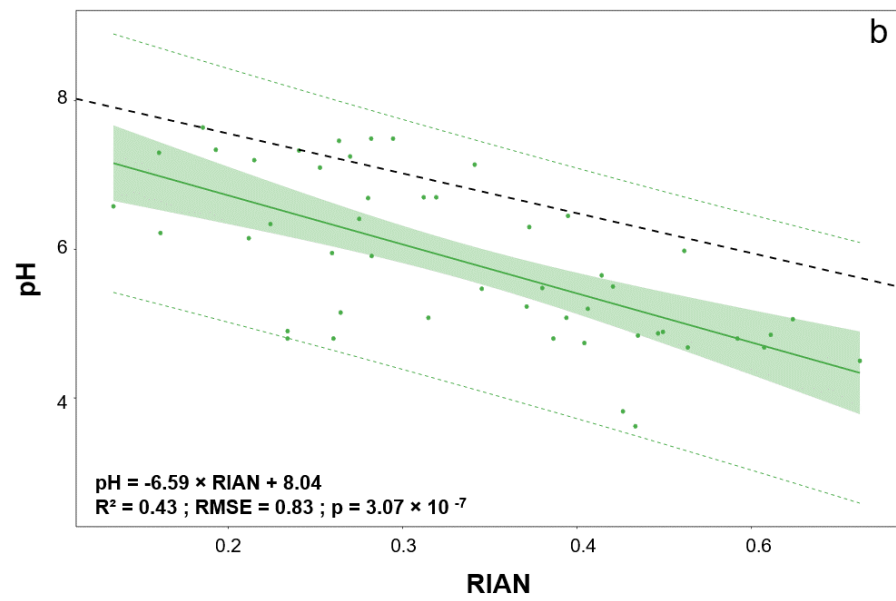
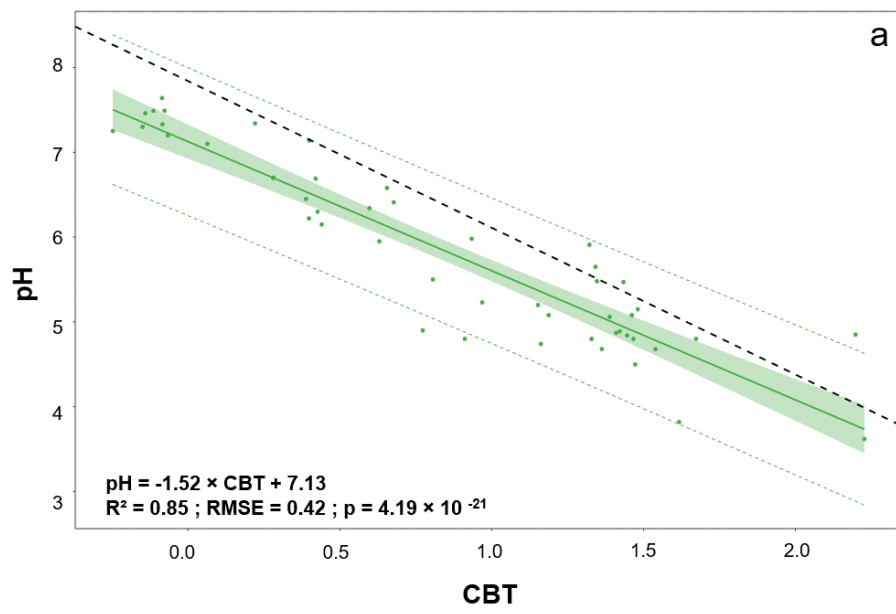


Figure 4

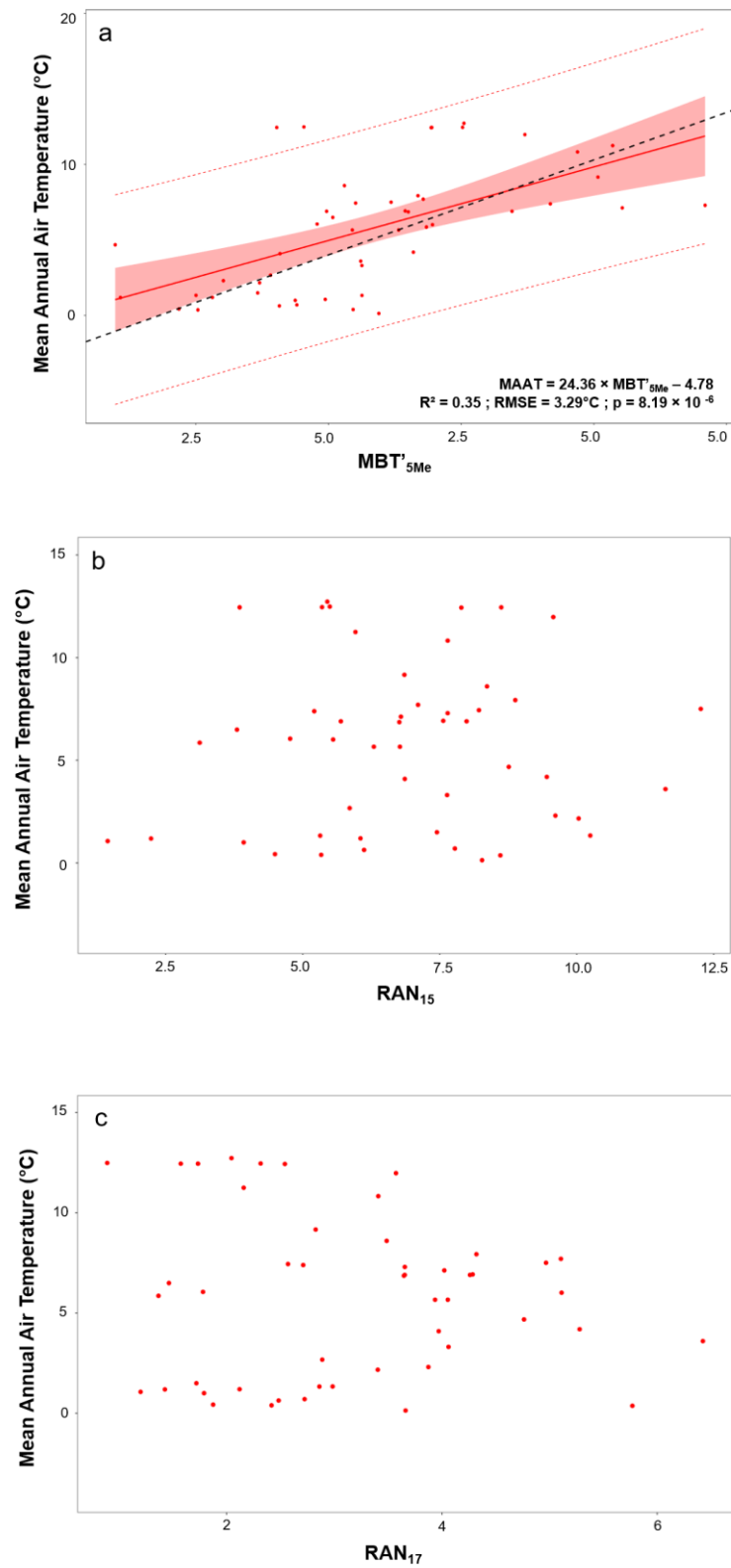


Figure 5

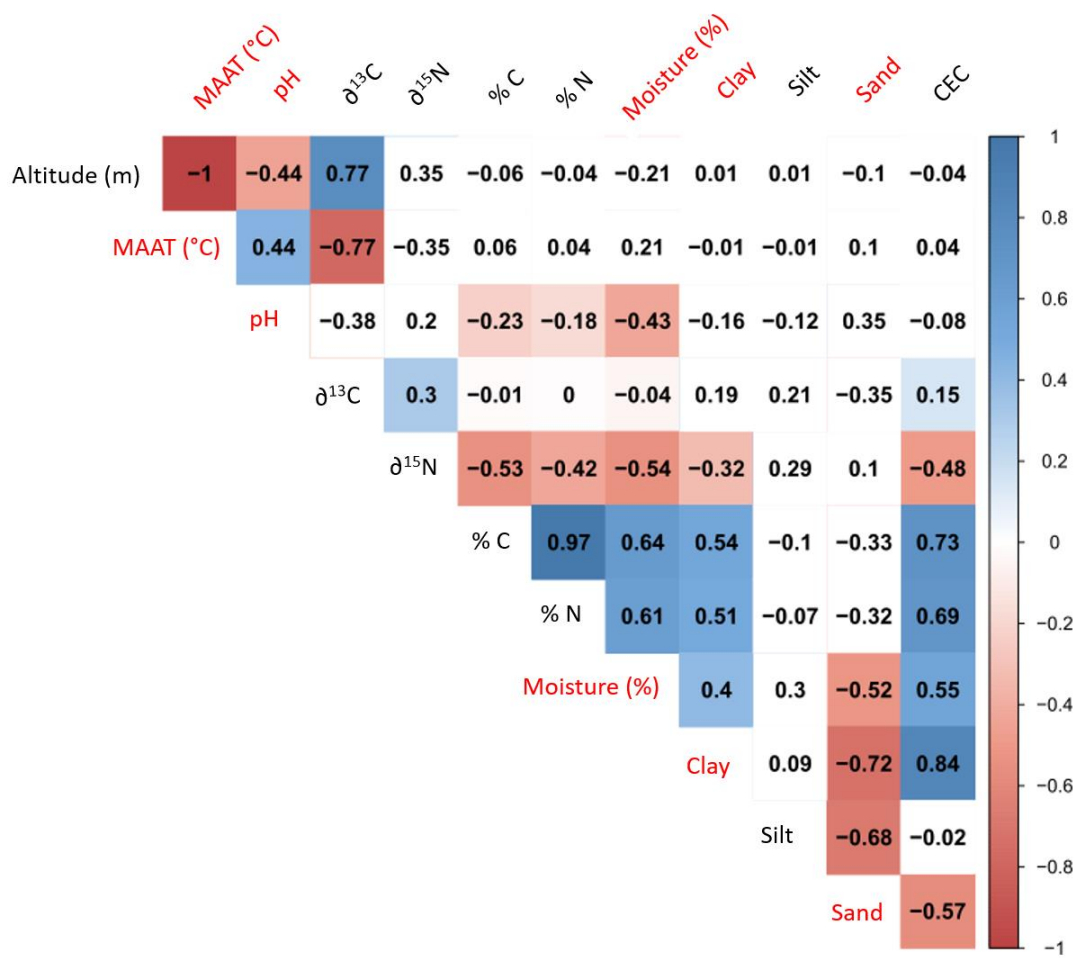
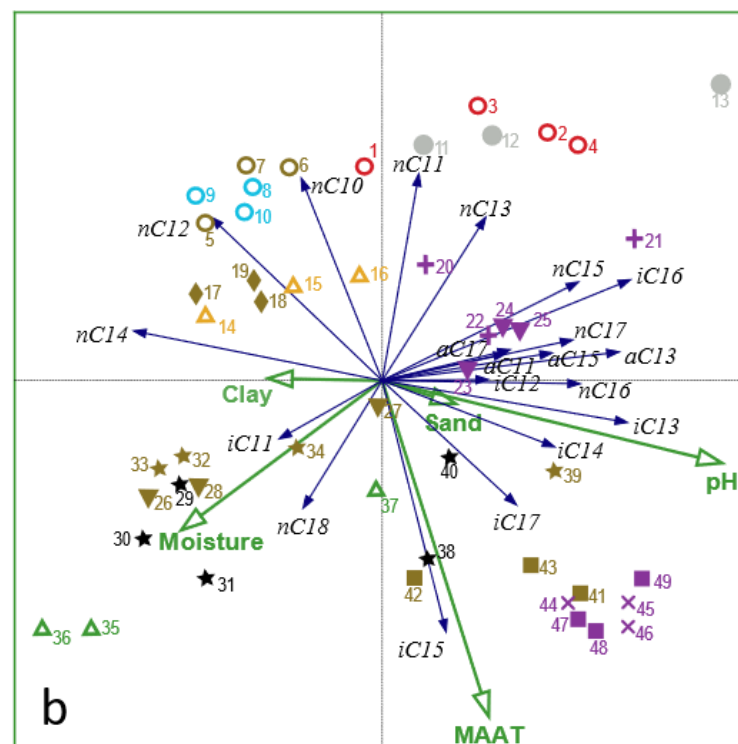
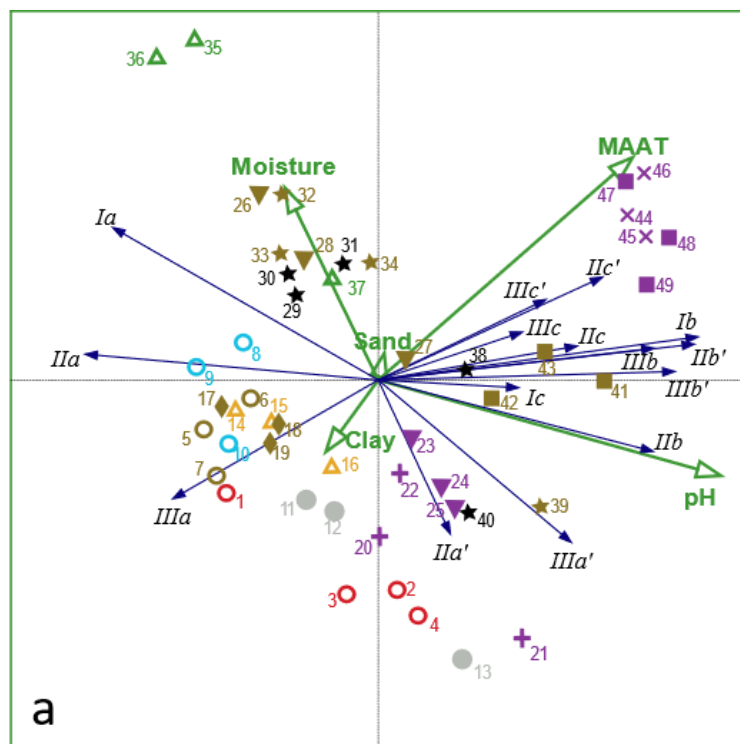


Figure 6



- Alpine meadow
- Rocks
- △ Heathlands
- ◆ Subalpine meadow
- + Subalpine forest
- ▼ Mountainous meadow
- ★ Mountainous forest
- Lowland meadow
- × Lowland forest
- Rendisol
- Brunisol
- Colluviosol
- Lithosol
- Alacrisol
- Calcosol
- Organosol
- Podzosol

Figure 7

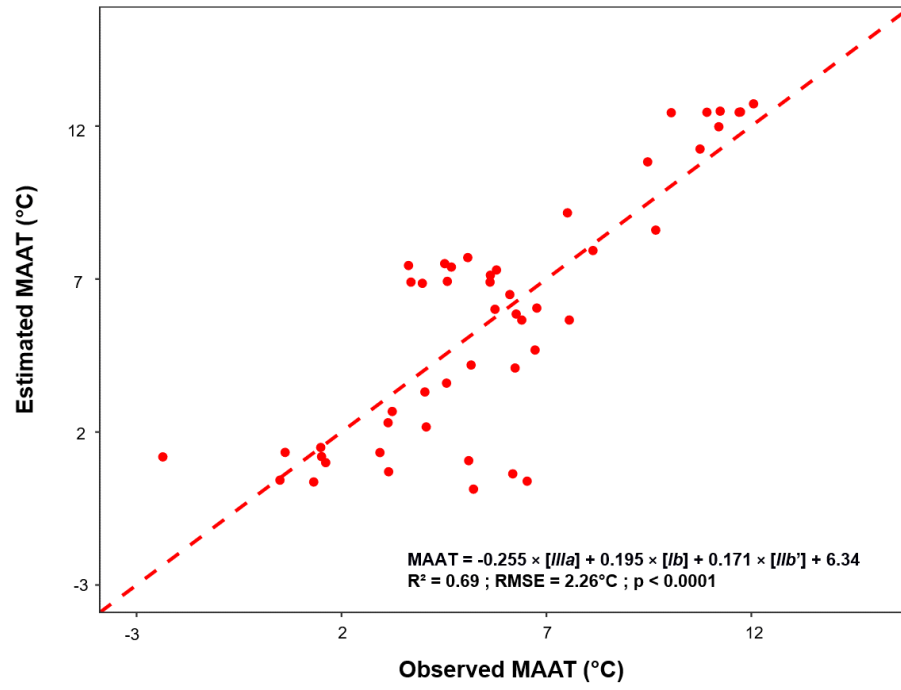


Figure 8

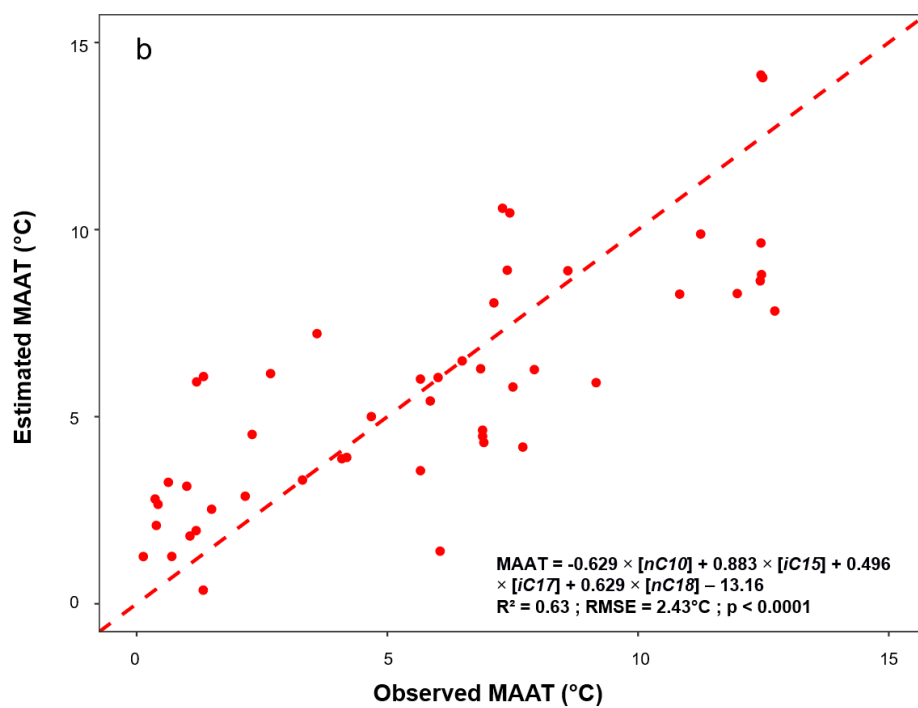
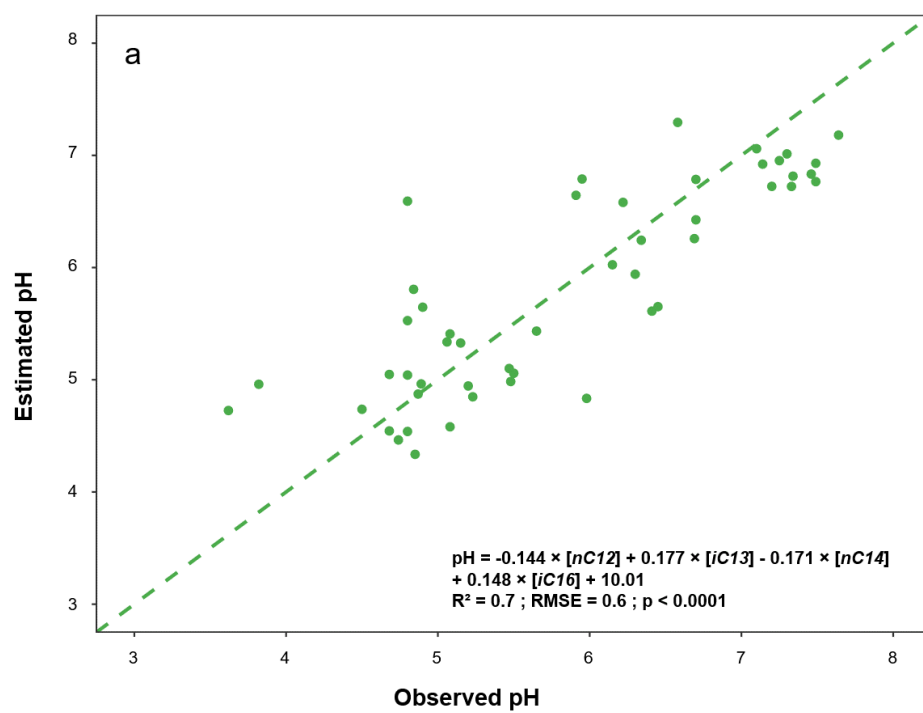


Figure 9

Samples	Massif	Coordinates	Altitude (m)	Soil Type	Vegetation
1	Lautaret	45° 3'35.24"N 6°23'30.96"E	2700	Rendisol	Alpine meadow (<i>Kobresia simpliciuscula</i>)
2		45° 3'35.24"N 6°23'30.96"E	2646	Rendisol	Alpine meadow (<i>Kobresia simpliciuscula</i>)
3		45° 3'36.04"N 6°21'54.02"E	2748	Rendisol	Alpine meadow (<i>Kobresia simpliciuscula</i>)
4		45° 3'32.98"N 6°22'4.63"E	2695	Rendisol	Alpine meadow (<i>Kobresia simpliciuscula</i>)
5		45° 3'15.48"N 6°24'3.11"E	2470	Brunisol	Alpine meadow (<i>Poa alpina</i>)
6		45° 3'29.19"N 6°22'22.86"E	2632	Brunisol	Alpine meadow (<i>Poa alpina</i>)
7		45° 3'33.77"N 6°22'9.07"E	2688	Brunisol	Alpine meadow (<i>Poa alpina</i>)
8		45° 3'0.43"N 6°23'6.15"E	2503	Colluviosol	Alpine meadow (<i>Carex foetida</i>)
9		45° 3'15.75"N 6°22'30.15"E	2571	Colluviosol	Alpine meadow (<i>Carex foetida</i>)
10		45° 3'13.32"N 6°22'41.51"E	2531	Colluviosol	Alpine meadow (<i>Carex foetida</i>)
11		45° 2'55.20"N 6°23'14.02"E	2504	Lithosol	Rocks
12		45° 3'1.99"N 6°22'54.88"E	2533	Lithosol	Rocks
13		45° 3'10.66"N 6°22'39.90"E	2558	Lithosol	Rocks
14		45° 2'38.94"N 6°24'8.20"E	2230	Alocrisol	Heathland (<i>Vaccinium myrtillus</i>)
15		45° 2'53.79"N 6°23'45.81"E	2305	Alocrisol	Heathland (<i>Vaccinium myrtillus</i>)
16		45° 2'59.32"N 6°23'32.53"E	2333	Alocrisol	Heathland (<i>Vaccinium myrtillus</i>)
17		45° 2'42.11"N 6°24'25.73"E	2100	Brunisol	Subalpine meadow(<i>Festuca paniculata</i>)
18		45° 2'26.05"N 6°25'8.51"E	1920	Brunisol	Subalpine meadow(<i>Festuca paniculata</i>)
19		45° 2'25.32"N 6°24'30.39"E	2041	Brunisol	Subalpine meadow(<i>Festuca paniculata</i>)
20		45° 2'22.35"N 6°26'6.73"E	1940	Calcosol	Subalpine forest (<i>Larix decidua</i>)
21		45° 1'33.34"N 6°27'8.63"E	1820	Calcosol	Subalpine forest (<i>Larix decidua</i>)
22		44°59'47.61"N 6°28'50.40"E	1620	Calcosol	Subalpine forest (<i>Larix decidua</i>)
23		45° 0'49.54"N 6°28'0.44"E	1620	Calcosol	Mountainous meadow
24		45° 0'4.78"N 6°28'27.34"E	1580	Calcosol	Mountainous meadow
25		44°59'39.52"N 6°28'43.30"E	1540	Calcosol	Mountainous meadow
26	Bauges	45°40'2.47"N 5°58'17.07"E	1475	Brunisol	Mountainous meadow
27		45°40'14.96"N 5°58'25.39"E	1450	Brunisol	Mountainous meadow
28		45°40'29.61"N 5°59'53.47"E	1360	Brunisol	Mountainous meadow
29		45°40'31.96"N 5°59'46.20"E	1375	Organosol	Mountainous forest
30		45°40'33.31"N 5°59'51.52"E	1367	Organosol	Mountainous forest
31		45°40'27.77"N 5°59'47.87"E	1362	Organosol	Mountainous forest
32		45°40'31.96"N 5°59'46.20"E	1375	Brunisol	Mountainous forest
33		45°40'33.31"N 5°59'51.52"E	1367	Brunisol	Mountainous forest
34		45°40'27.77"N 5°59'47.87"E	1362	Brunisol	Mountainous forest
35		45°38'20.27"N 5°59'36.04"E	1286	Podzosol	Heathland (<i>Vaccinium myrtillus</i>)
36		45°38'43.73"N 5°59'26.42"E	1314	Podzosol	Heathland (<i>Vaccinium myrtillus</i>)
37		45°38'47.71"N 5°59'24.09"E	1321	Podzosol	Heathland (<i>Vaccinium myrtillus</i>)
38		45°40'22.12"N 5°57'43.67"E	905	Organosol	Mountainous forest (<i>Fagus sylvatica</i>)
39		45°40'17.69"N 5°57'44.82"E	938	Brunisol	Mountainous forest (<i>Fagus sylvatica</i>)
40		45°40'6.46"N 5°57'41.22"E	1017	Organosol	Mountainous forest (<i>Fagus sylvatica</i>)
41		45°40'48.07"N 5°56'30.30"E	462	Brunisol	Lowland meadow
42		45°40'47.24"N 5°57'1.91"E	565	Brunisol	Lowland meadow
43		45°40'52.82"N 5°56'52.87"E	520	Brunisol	Lowland meadow
44		45°38'53.89"N 5°52'3.84"E	232	Calcosol	Lowland forest (<i>Fraxinus excelsior</i>)
45		45°38'51.44"N 5°52'3.85"E	234	Calcosol	Lowland forest (<i>Fraxinus excelsior</i>)
46		45°38'9.90"N 5°52'9.58"E	237	Calcosol	Lowland forest (<i>Fraxinus excelsior</i>)
47		45°38'54.08"N 5°51'58.44"E	232	Calcosol	Lowland meadow (<i>Carex foetida</i>)
48		45°38'59.87"N 5°52'0.01"E	232	Calcosol	Lowland meadow (<i>Carex foetida</i>)
49		45°38'22.21"N 5°52'12.53"E	234	Calcosol	Lowland meadow (<i>Carex foetida</i>)

Table 1

Samples	MAAT (°C)	pH	C org (%)	N (%)	δ ¹³ C	δ ¹⁵ N	Moisture (%)	Clay (g/kg)	Silt (g/kg)	Sand (g/kg)	CEC (cmol +/-kg)
1	0.4	5.1	3.8	0.31	-25.9	2.8	12.4	112	207	681	49.1
2	0.6	6.3	6.2	0.59	-25.4	3.0	27.5	273	411	316	22.6
3	0.1	6.0	5.9	0.57	-24.4	6.7	22.7	312	438	250	21.4
4	0.4	6.5	12.7	1.22	-24.9	2.8	39.4	323	407	270	38.3
5	1.5	4.7	7.0	0.62	-25.4	3.6	29.5	380	457	163	20.8
6	0.7	4.9	5.0	0.46	-25.1	4.3	30.3	290	579	131	16.1
7	0.4	4.9	7.7	0.59	-25.6	2.1	28.9	385	467	148	21
8	1.3	4.8	2.0	0.21	-25.0	4.0	26.0	248	623	129	10.3
9	1.0	4.5	4.1	0.37	-25.2	3.7	31.4	321	557	122	13.4
10	1.2	4.8	7.3	0.56	-25.7	8.5	34.1	378	461	161	19.2
11	1.3	5.7	2.0	0.18	-26.3	4.2	8.6	197	423	380	9.48
12	1.2	5.9	1.4	0.15	-25.7	4.2	9.1	136	381	483	8.27
13	1.1	7.1	1.5	0.16	-25.4	1.9	3.4	115	310	575	5.98
14	2.7	4.7	17.8	1.10	-25.8	-0.2	45.8	448	406	146	31.9
15	2.3	5.1	13.6	0.81	-25.3	0.0	44.8	368	405	227	28.6
16	2.2	5.5	17.7	1.22	-25.0	2.0	52.9	432	444	124	47.5
17	3.3	4.8	9.1	0.71	-25.5	2.9	26.3	416	424	160	23.5
18	4.2	5.2	5.9	0.50	-26.1	2.5	16.6	377	420	203	20.4
19	3.6	5.2	6.6	0.58	-25.4	3.3	22.9	412	428	160	23.1
20	4.1	6.2	6.5	0.57	-25.7	1.7	16.0	395	392	213	24.6
21	4.7	7.3	6.3	0.54	-25.7	2.6	12.2	385	399	216	19.4
22	5.7	6.3	5.1	0.34	-27.4	1.7	5.8	194	232	574	13.2
23	5.7	6.2	9.4	0.78	-27.0	1.2	23.9	254	299	447	24.6
24	5.9	6.6	7.5	0.64	-26.9	3.2	11.7	277	341	382	23.3
25	6.1	6.7	5.8	0.56	-26.4	4.2	13.6	350	381	269	20.2
26*	7.5	4.7	3.1	0.28	-26.7	1.1	31.8	321	443	236	15.8
27	6.5	6.0	3.8	0.40	-26.9	5.1	33.1	344	457	199	21
28*	7.4	5.1	5.9	0.53	-26.2	1.0	35.6	396	434	170	23.1
29*	6.0	4.9	32.9	1.89	-26.7	-5.0	61.7	513	458	29	74.7
30	6.9	4.8	49.1	2.10	-25.1	-2.50	64.7	540	428	32	64.3
31*	7.7	5.2	41.0	2.03	-39.9	-3.8	68.2	546	452	2	96
32	6.9	4.8	4.7	0.33	-25.6	-1.0	33.7	305	525	170	21.5
33	6.9	4.9	6.4	0.49	-26.5	0.0	36.4	398	458	144	26.9
34	6.9	5.5	6.8	0.42	-25.2	-0.8	39.9	345	541	114	30.5
35	7.3	3.8	29.0	1.37	-27.7	-1.8	62.7	114	191	695	11.5
36*	7.4	3.6	31.0	1.74	-28.8	-1.5	53.4	98	100	802	13.2
37	7.1	5.5	2.4	0.12	-27.9	-0.3	21.0	33	98	869	8.05
38	9.2	6.4	19.8	1.05	-27.9	-2.7	46.4	411	285	304	32.9
39*	8.6	7.2	11.6	0.88	-26.5	-1.0	28.0	432	304	264	34.7
40*	7.9	6.7	5.8	0.39	-27.1	-0.6	30.4	516	294	190	35.8
41*	12.0	7.5	8.7	0.86	-27.1	2.3	23.3	357	329	314	24.7
42	10.8	6.7	4.3	0.35	-28.4	-0.2	26.1	477	314	209	28.4
43*	11.2	7.1	1.7	0.18	-25.9	7.0	17.5	276	330	394	17.8
44*	12.5	7.3	5.2	0.53	-27.9	2.9	26.8	227	577	196	11.8
45	12.5	7.5	7.3	0.69	-28.0	1.9	26.5	181	510	309	10.8
46	12.4	7.3	2.7	0.24	-29.4	1.3	31.6	95	501	404	9.65
47*	12.7	7.3	2.2	0.23	-28.3	5.0	27.2	171	559	270	9.02
48	12.5	7.5	9.8	0.90	-28.7	2.2	47.2	327	599	74	26.9
49	12.5	7.6	2.4	0.21	-27.7	6.2	16.0	175	434	391	7.32

Table 2

Variables	brGDGTs		3-OH FAs	
	Axis 1	Axis 2	Axis 1	Axis 2
pH	0.96	-0.26	0.95	0.23
MAAT (°C)	0.71	0.62	0.29	-0.93
Moisture (%)	-0.26	0.53	-0.56	-0.41
Clay (g/kg)	-0.14	-0.2	-0.32	0.006
Sand (g/kg)	0.02	0.08	-0.21	-0.06
Expl. variation (%)	44.09	6.13	21.27	10.51
Expl. fitted variation (%)	78.47	10.91	54.39	26.84

Table 3

Variables	brGDGTs		3-OH FAs	
	Simple effets (%)	Conditional effects (%)	Simple effets (%)	Conditional effects (%)
pH	41.1 ***	41.1***	20.0 ***	20.0 ***
MAAT (°C)	25.2 ***	8.1 ***	11.2 **	10.9 ***
Moisture (%)	5.3 *	1.5 °	9.9 ***	3.6*
Clay (g/kg)	2.8	2.0 *	3.8°	2.5 °
Sand (g/kg)	1.4	3.5 **	2.1	2.2

Table 4